HHS Public Access

Author manuscript

Chem Mater. Author manuscript; available in PMC 2017 May 12.

Published in final edited form as:

Chem Mater. 2011 ; 23(3): 483–500. doi:10.1021/cm1021905.

Metal Ion-Responsive Fluorescent Probes for Two-Photon Excitation Microscopy

S. Sumalekshmy and **Christoph J. Fahrni***

School of Chemistry and Biochemistry and Petit Institute for Bioengineering and Bioscience, Georgia Institute of Technology, 901 Atlantic Drive, Atlanta, Georgia 30332

Abstract

Metal ion-responsive fluorescent probes are powerful tools for visualizing labile metal ion pools in live cells. To take full advantage of the benefits offered by two-photon excitation microscopy, including increased depth penetration, reduced phototoxicity, and intrinsic 3D capabilities, the photophysical properties of the probes must be optimized for nonlinear excitation. This review summarizes the challenges associated with the design of two-photon excitable fluorescent probes and labels and offers an overview on recent efforts in developing selective and sensitive reagents for the detection of metal ions in biological systems.

1. Introduction

According to current estimates approximately 40% of the proteome is composed of proteins that require one or multiple metal ions for their proper function. Given the complex chemical composition of a cell or organism, a sophisticated machinery is required to guarantee the faithful insertion of metal ions into the respective metalloproteins. Although numerous genes and proteins have been identified that are involved in metal trafficking pathways, still little is known about the subcellular distribution and speciation of metal ions during normal cell function and alterations in specific diseases. Considering the small size of a single cell, it is apparent that the in situ detection of metal ions requires very sensitive microanalytical techniques with high spatial resolution. Among suitable imaging modalities, visible-light fluorescence microscopy is presumably the most cost-effective technique. It offers not only submicron spatial resolution but also excellent sensitivity down to the single molecule level. Because the biologically relevant metal ions are not fluorescent, a reporter molecule must be introduced that selectively binds to the metal ion of interest and signals its presence through a change in emission intensity or color. Because such a fluorescent indicator inevitably competes with other endogenous ligands for metal binding, this approach is not suitable to analyze the total metal ion content of a cell. Nevertheless, in the context of exploring metal ion trafficking pathways and signaling events, the metal ions of interest are inherently labile, and therefore, this apparent limitation becomes in fact a desirable feature for selectively probing this exchangeable metal pool. For example, fura-2, one of the first fluorescence metal indicators developed for the detection of Ca(II) ions in live cells, has revolutionized the understanding of Ca(II)-mediated signaling in neurobiology. Spurred by this initial

Phone: 404-385-1164/fax: 404-894-2295, fahrni@chemistry.gatech.edu.

success, many fluorescent indicators have since been developed for the detection of a broad range of metal ions, including even toxic heavy metals such as Hg(II), Pb(II), and Cd(II).,

Over the past decade, the capabilities of fluorescence-based biological imaging have been further expanded by two-photon excitation microscopy (TPEM).– Originally invented by Webb and coworkers, this technique utilizes an ultrafast pulsed laser as excitation source, which leads to the simultaneous absorption of two photons by the fluorophore. Consequently, the excited state of a fluorophore can be accessed by absorption of two photons of half the energy compared to the one-photon process. Hence, many popular fluorophores used in bioimaging can be excited in the near-infrared region, which offers improved depth penetration in scattering media and reduced photo toxicity. Furthermore, two-photon absorption scales linearly with the squared intensity of the laser beam, such that excitation occurs only within a spatially confined volume at the focal point of the microscope objective. By acquiring images at equally spaced positions across the vertical axis of the specimen, a three-dimensional volume rendering can be constructed. These properties rendered this technique particularly attractive for biological imaging, and more recently, stimulated also the development of fluorescent metal ion indicators tailored towards TPEM applications. This review is intended to provide an overview of these recent efforts with an emphasis on the underlying photophysical principles used for the design of such metal responsive indicators.

2. Design Strategies for Cation-Responsive Fluorescent Indicators

2.1. General Principles

Depending on the mode of fluorescence response, metal-ion indicators can be divided into two major classes. The first group undergoes a change in fluorescence intensity, either an increase or decrease upon binding of the metal ion, whereas the second group responds with a chromatic shift of the peak emission. Assuming a 1:1 stoichiometry for the complex formed between metal ion and indicator, the measurement of the fluorescence intensity F is principally sufficient to determine the free metal ion concentration according to equation (1)

$$[M^{n+}]=K_d\left(\frac{F-F_{\min}}{F_{\max}-F}\right), \quad (1)$$

where K_d is the dissociation constant of the metal-indicator complex, and F_{min} and F_{max} are the minimum and maximum fluorescence intensities for the free and saturated probe, respectively, typically obtained from calibration experiments with metal-buffered solutions at a fixed indicator concentration. Because the latter may vary strongly from cell to cell and even within different regions of the cytoplasm, it is difficult to utilize fluorescence intensity measurements to obtain reliable quantitative information of intracellular metal pools. The data interpretation is further complicated through time-dependent photobleaching or accumulation of the indicator to intracellular compartments. These problems can be circumvented with indicators that undergo a spectral shift upon analyte binding. By measuring the ratio R of the fluorescence intensities at two excitation or emission

wavelengths, the probe response can be directly related to the free metal ion concentration according to

$$[M^{n+}]=K_d\left(\frac{R-R_{\min}}{R_{\max}-R}\right)\left(\frac{S_f}{S_b}\right), \quad (2)$$

where K_d is again the dissociation constant of the metal-probe complex (with 1:1 stoichiometry), R_{min} and R_{max} are the minimum and maximum intensity ratios for the free and saturated probe, and S_f and S_b are instrument dependent calibration constants. In this case, fluorescence intensity differences due to uneven distribution, photobleaching, relocalization, or instrument dependent fluctuations are cancelled out. It is important to note that the ratiometric approach is still not entirely devoid of artifacts. Because the intensity ratio R reflects the fractional saturation of the indicator by the analyte, the indicator concentration should remain below the total amount of available analyte.

While the limit of detection for both indicator classes depends, in the first place, on the thermodynamic affinity towards the metal cation of interest, the optical sensitivity relies on the brightness and detectability of the fluorescence change. Because it is easier to differentiate small differences in intensity rather than spectral changes, the dynamic range of intensity-based indicators is naturally larger, which may be particularly advantageous when attempting to monitor low analyte concentrations. In this sense, one type of indicator is not necessarily better than the other; each offers a distinct set of advantages and disadvantages that must be balanced in context of the application at hand. Regardless of the response mode, both indicator classes rely on efficient two-photon absorbing fluorophores that can be readily detected by TPEM. For this reason, we start our discussion with an overview of design strategies of two-photon absorbing fluorophores geared towards biological applications.

2.2. Two-Photon Absorbing Fluorophores

Although fluorescent dyes and indicators commonly used in linear microscopy can be also applied in TPEM (see also section 3), there are two potential limitations. First, the fluorophore brightness, which is proportional to the fluorescence quantum yield and absorption cross section, may be compromised due to a low 2PA cross section. While the quantum yield is typically assumed to be independent of the excitation mode, the cross section follows different quantum mechanical rules for the nonlinear two-photon compared to one-photon process. Optimizing the two-photon absorption cross section is therefore critical to improving the optical sensitivity of organic fluorophores for TPEM. Second, the majority of ratiometric fluorescent probes commonly used in biological research undergo only a shift in the excitation but not emission profile. Given the significant costs of femtosecond-pulsed lasers, TPEM is restricted to a single excitation source, and for this reason, ratiometric probes that require rapid switching between two excitation wavelengths are not practical for TPEM.

A number of strategies have been identified to maximize the 2PA cross section of fluorophores.– From a fundamental point of view, the 2PA cross section is proportional to the imaginary part of the second hyperpolarizability

$$\delta(\omega) \propto \mathrm{Im}[\gamma(-\omega;\omega,\omega,-\omega)]. \quad (3)$$

On a molecular level, $\delta(\omega)$ can be maximized by combining three distinct structural elements: electron donating groups (D), electron accepting groups (A), and conjugated π-bridges that connect the donor and acceptor components. As illustrated with Figure 1, depending on their spatial arrangement, simple dipolar (a), symmetrical quadrupolar (b), or more complex octupolar structures (c) can be envisioned. Moreover, the architectures are not limited to two-dimensional arrangements, but can be further expanded to complex 3D designs. Despite the structural diversity, all of these architectures are devoted towards maximizing the degree of charge transfer upon photoexcitation while maintaining a strong transition dipole moment.

The structure-property relationships for the various design approaches have been extensively reviewed;– therefore, the following section only focuses on the key concepts and a few selected examples geared towards bioimaging.

2.2.1. Noncentrosymmetric Dipolar Fluorophores—The attachment of an electron-rich donor and an electron deficient acceptor group to a linear π-system typically results in an uneven, dipolar ground state charge distribution. Upon photoexcitation, such dipolar fluorophores undergo charge redistribution from the donor to the acceptor group to give a further polarized excited state with an increased dipole moment compared to the ground state. Applying a simplified two state model that only includes the electronic ground state S_0 and the lowest excited state S_1,, the peak cross section δ_{max} at the two-photon resonance energy ($2h\nu = E_1$) is related to the transition dipole moment M_{01} and the change in permanent dipole moment $\Delta\mu = \mu_1 - \mu_0$ between ground and excited state according to equation (4)

$$\delta_{\max} = \frac{2\pi L^4}{5\varepsilon_0^2 n^2 c^2 h} \frac{(\Delta\mu)^2 M_{01}^2}{\Gamma} \ (\text{in SI units}), \quad (4)$$

where Γ corresponds to a damping factor that represents the overall bandwidth of the $S_0 \rightarrow S_1$ transition. The enhancement of the optical field in the medium relative to vacuum is described by $L = (n^2+2)/3$, where n is the refractive index of the medium. The cross section δ is typically reported in units of Göppert-Mayer (1 GM = 10^{-50} cm^4 s/photon), giving tribute to Maria Göppert-Mayer who developed the theory of two-photon absorption in the 1930s. From equation (4) it becomes evident that the two photon cross section increases with increasing charge transfer in the excited state, which is typically achieved by increasing the donor and acceptor strength of the terminal substituents. As the difference between

donor and acceptor strength is increasing, the ground state increasingly resembles the charge-separated zwitter-ionic resonance structure **II** as illustrated with a simple D-A substituted stilbene π-system.

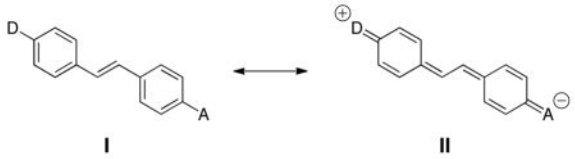

If both resonance structures **I** and **II** contribute equally to the ground state, the so-called cyanine limit is reached for which the degree of π-bond alteration (BOA) is vanishingly small. Theoretical studies showed that the 2PA cross section peaks at an intermediate value of BOA; however, at such values the associated excitation energy E_1 is very low and typically lies outside the spectral window of the Ti-sapphire laser used in TPEM. For this reason, finding the optimal combination of donor and acceptor strength for a given π-system is critical for maximizing the 2PA cross section of dipolar fluorophores for TPEM applications.

Figure 2 shows a compilation of dipolar fluorophores that have been specifically developed as labels for biological multiphoton imaging. By using a fluorene core to bridge a diphenyl amino donor moiety and an electron deficient benzothiazole acceptor, a 2PA cross section of 202 GM (λ = 780 nm) was achieved with fluorophore **1a** (Table 1). The utility of **1** for TPEM was demonstrated with rat cardiomyoblast cells, which showed predominantly cytoplasmic staining upon incubation with the dye. To explore the utility of **1a** as biolabel, an amine reactive derivative **1b** was synthesized and conjugated to bovine serum albumin (BSA). Featuring a further extended conjugation length, the 2PA cross section of fluorophores **2a** and **2b** improved to 248 GM (λ = 730 nm) and 563 GM (λ = 730 nm), respectively. Incubation of COS-7 and HCT 116 cells with **2a** revealed a punctate staining pattern with a predominantly endosomal localization (Figure 3).

Similar to **2b**, chromophores **3a-c** feature also a fluoroethynyl bridge to link a dialkylamino donor group with a range of pyridine dicarboxamide derivatives as electron acceptors., In dichloromethane, the parent compound **3a** exhibits a large 2PA cross section of 1146 GM (λ = 830 nm). The attachment of hydrophilic substituents in **3b** and **3c** produced amphiphilic probes suitable for biological imaging. Whereas incubation of CHO cells with **3b** yielded predominant staining of the plasma membrane, the pyrasonide substituted dye **3c** readily crossed the cell membrane and revealed a cytoplasmic staining. The 2H-Benzo[h]chromene-2-one core of derivatives **4** efficiently integrates a donor-acceptor pair in a co-planar orientation which facilitates the charge redistribution in the excited state. Depending on the nature of the acceptor, fluorophores **4a** and **4b** offer large 2PA cross sections of 350 (λ = 880 nm) and 470 GM (λ = 940 nm), respectively. Incubation of A431 cells with **4a** showed rapid internalization and negligible toxicity, rendering **4a** suitable for live cell imaging studies. To explore the utility of this fluorophore as a chemical tag for two-photon imaging in live cells, Cornish and coworkers synthesized the cell permeant conjugate **5** (TMP-BC575) containing a trimethoprim moiety (TMP) as targeting group. The TMP-

modified fluorophore specifically binds to *E. coli* dihydrofolate reductase (eDHFR), a small 18kD protein that was expressed in HEP293 cells as fusion protein with a nuclear targeting sequence. Two-photon imaging with excitation at 940 nm revealed the exclusive localization of the label to cell nuclei. Despite having only a small conjugated **π**-system, the 1,5-disubstituted naphthalene derivative **6** showed a remarkably high 2PA cross section of 92 GM (λ = 720 nm) in DMSO as solvent. Detailed cellular studies with Hep3B cancer cells revealed that **6** is cell permeant and capable of inducing apoptosis in a dose-dependent manner. It is important to note that all fluorophores exhibit significantly lower action cross sections in polar solvents such as DMSO or water (Table 1). With increasing solvent polarity, solvent-solute interactions become more prominent and offer non-radiative deactivation pathways that reduce the fluorescence quantum yield and thus brightness of dipolar fluorophores.

2.2.2 Centrosymmetric Quadrupolar Fluorophores—In centrosymmetric fluorophores, two-photon excitation from the ground state S_0 to the lowest excited state S_1 is forbidden by dipole selection rules. Instead, the next higher excited state S_2 can be accessed through a non-stationary “virtual” state. The two-photon cross section of this type of fluorophore can be approximated with a three state model that includes the relevant states S_0, S_1 and S_2., Denoting the transition energies from the ground to the lowest excited and two-photon state as E_1 and E_2, respectively, the peak cross section δ_{max} at the two-photon resonance energy ($2h\nu = E_2$) can be expressed as a function of the transition dipole moments M_{01} and M_{12} according to equation (5)

$$\delta_{\max}=\frac{2\pi h\nu^2 L^4}{5\varepsilon_0^2 n^2 c^2}\frac{M_{01}^2 M_{12}^2}{(E_1-h\nu)\Gamma}\ (\text{in SI units}), \quad (5)$$

where Γ corresponds again to the damping factor that represents the overall bandwidth (full width at half-maximum) of the two-photon $S_0 \rightarrow S_2$ transition. For many quadrupolar organic chromophore, Γ can be approximated with ≈ 0.1 eV. Because all static dipole moments are zero in a centrosymmetric D-A architecture, the dipole term as expressed by equation (4) remains absent.

According to equation (5), structural modifications that increase the transition dipole moments M_{01} and M_{12} are expected to greatly increase the 2PA cross section. For example, the attachment of electron donating dibutylamino groups to stilbene **7** led to a nearly 20-fold increase of the 2PA cross section in **8**, a landmark discovery that set the foundation for the rational design of 2PA fluorophores based on structure-property relationships.

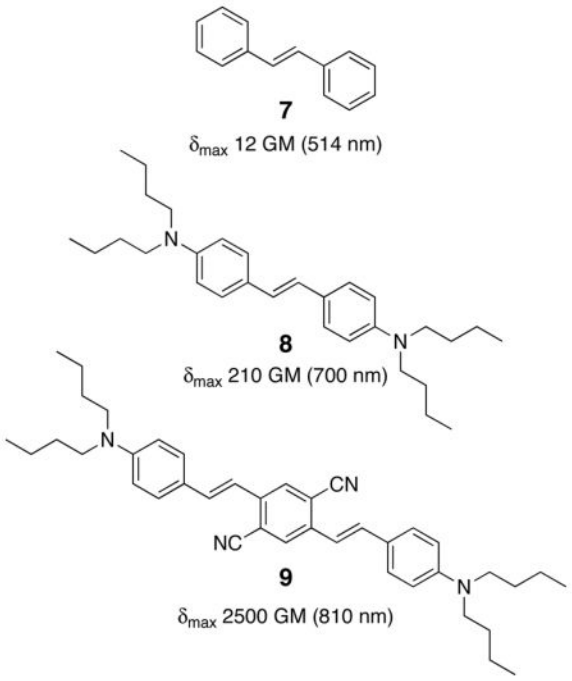

Quantum chemical calculations of **7** and **8** showed that M_{01} and M_{12} indeed increased from 7.1 to 8.8 D and 3.1 to 7.2 D, respectively. In addition, the donor substituents also exerted a favorable influence on the one-photon detuning term (E_1-hν), which decreased from 1.8 to 1.5 eV, and thus contributed to the enhanced δ. Extension of the conjugation length and addition of electron withdrawing cyano substituents in fluorophore **9** yielded a 2PA cross section that was further enhanced by two orders of magnitudes compared to the parent compound **7**. Since the initial discovery that centrosymmetric architectures can yield very large 2PA cross sections, a large number of quadrupolar two-photon fluorophores have been described, typically composed of two terminal donor or acceptor groups that are bridged through a conjugated π-system.,

Given the large 2PA cross sections that can be achieved with a centrosymmetric arrangement of donor and acceptors, quadrupolar fluorophores should be well suited as labels for TPEM; however, as already noted for dipolar fluorophores, the action cross section also decreases for this fluorophore architecture substantially in polar solvents. Nevertheless, a number of quadrupolar fluorophores have been successfully developed as labels for biological multiphoton imaging (Figure 4). For example, **10a** exhibits a maximum 2PA cross section of 160 GM (λ = 720 nm) in aqueous solution., Taking into account the excellent quantum yield of 0.72, this fluorophore is more than three times brighter compared to fluorescein. To improve the water solubility, the conjugated hydrocarbon core was functionalized with multiple oligoethyleneglycol chains. Despite the considerable molecular weight of 1.4 kD, **10a** was readily taken up into live cells within 10 minutes and produced a perinuclear staining pattern. For comparison, the structurally related label **10b** containing a biphenyl core exhibits both a lower 2PA cross section and quantum yield, thus underscoring the importance of a co-planar conjugatedπ-system with restricted conformational freedom., Fluorophores **11a** and **11b** contain a non-conjugated pyrazobole core, which could be

readily utilized for the design of other centrosymmetric donor-donor 2PA systems. The boron containing moiety might serve as a building block of bifunctional molecules as labels for TPEM imaging and sensitizers for boron neutron capture therapy (BNCT). Despite their lipophilicity, both fluorophores were rapidly internalized by HeLa cells and displayed vesicular staining and some residual cytosolic fluorescence (Figure 5). Fluorescence lifetime imaging studies revealed a decay time that was comparable to organic solvents, indicating a hydrophobic cellular environment.

Structurally related to the dipolar fluorophores **2** and **3**, centrosymmetric **12b** also showed a substantially increased 2PA cross section compared to **12a** due to the additional conjugation length provided by the alkynyl spacers. Presumably due to aggregation effects, the 2PA efficiency of **13a** in water was up to three times higher compared to aprotic solvents. Conjugation with a cyclic peptide RGDfK yielded **13b** which selectively targeted integrin glycoproteins located at the plasma membrane. Composed of a [2.2]paracyclophane core to bridge two distrylbenzene fragments, an exceptionally high 2PA cross section around 700 GM (λ = 700 nm)was achieved with fluorophore **14** in aqueous solution. The study also demonstrated that the 2PA cross section does not necessarily increase with stronger donor substituents. In fact, weaker donors appear to be the better choice for applications in polar solvents, since the reduced dipole strength of the excited fluorophore results in weaker solvent-solute interactions, thus improving the quantum yield and overall brightness.

2.2.3. Metal Complexes—A range of metal ions has been utilized as templates to assemble a variety of three-dimensional multipolar structures (Figure 6). The electropositive metal center can induce strong intraligand charge transfer states with increased polarization compared to the free ligand. Following this design approach, the bis-cinnamaldiminato Schiff base Zn(II) complex **15** was synthesized and exhibited a very large 2PA cross sections around 10,000 GM (λ = 890 nm). Because the 2PA properties of **15** were determined by the open-aperture Z-scan technique, an approach that tends to enhance the apparent 2PA cross section due to excited state absorption (ESA) or thermal lens effects, a direct comparison with data obtained from two-photon excited fluorescence measurements is difficult. Theoretical investigations demonstrated a direct dependence of 2PA cross section on the Lewis acidity of the metal center used for complex formation. By using a donor-substituted bipyridine as ligand, the octupolar complexes **16a** and **16b** were assembled. Compared to the free ligands, the Zn(II) complex exhibited an almost 3-fold increase of the 2PA cross section from 69 (λ = 760 nm) to 214 GM (λ = 895 nm) in case of **16a**, and from 190 (λ = 730 nm) to 530 GM (λ = 820 nm) for **16b**. Independent investigations of the photophysical properties of **16a** revealed even larger values of 860 GM (λ = 965 nm), determined by the Z-scan technique, and 1018 GM (λ = 900 nm) according to two-photon excited fluorescence measurements. Compared to the free ligand, the 2PA cross section of the terpyrdine Zn(II) complex **18** increased 2-fold from 96 GM to 186 GM. Consistent with strongly increased excited state polarization upon Zn(II) coordination, the emission maximum shifted to lower energy from 413 nm to 549 nm in toluene as solvent. The tridentate ligands **17a** and **17b** formed well-defined complexes with 1:2 metal-ligand stoichiometry with a range of metal ions. Compared to the free ligands, the 2PA cross sections were strongly enhanced and

reached maxima of 2600 (λ = 800 nm) and 2730 GM (λ = 850 nm) in case of the Zn(II) complexes with ligands **17a** and **17b**, respectively.

Despite the large 2PA cross sections that were achieved through metal-enhanced excited state polarization, the kinetic lability of the metal complexes, especially in case of Zn(II), Ca(II), and Mg(II), precludes their application as biolabels. More recently, octupolar lanthanide complexes have been reported that are sufficiently stable in aqueous solution, thus offering an attractive avenue for developing new labels for biological TPEM., For example, the water-soluble Eu(III) complex with ligand **19** showed 2PA cross section of 92 GM (λ = 700 nm) and was successfully loaded into fixed T24 cancer cells (Figure 7).

2.3. Metal-Responsive Fluorescent Probes

To design a metal-responsive fluorescent indicator for TPEM, the fluorescence output of a two-photon absorbing fluorophore must be manipulated in a metal-dependent manner. This can be principally accomplished in two different ways; either by influencing the 2PA cross section upon metal binding or by altering the course of excited state deactivation pathways. In the first case, metal binding would typically affect both the intensity and wavelength of the fluorescence emission, whereas in the second scenario only the fluorophore brightness would be altered.

2.3.1. Photoinduced Charge Transfer Probes (PCT)—The terminal electron donating groups of dipolar and quadrupolar two-photon absorbing molecules discussed above offer a convenient way to directly integrate a metal binding site into the fluorophore structure. Because the excited state polarization and degree of charge transfer depend on the donor strength, metal ion binding is expected to directly influence both, the 2PA cross section and emission properties, of the fluorophore. This design strategy should be therefore suitable for the construction of simple intensity responsive probes as well as ratiometric indicators that undergo a spectral shift upon metal binding.

Examples of centrosymmetric and pseudo-centrosymmetric metal-responsive indicators with a D-π-A-π-D scaffold are depicted in Figure 8 and their photophysical data are compiled in Table 3. In the absence of metal cations indicator **20** exhibits a 2PA cross section comparable to the dibutylamino substituted parent compound **9**; however, upon saturation with Mg(II) ions the cross section at 810 nm decreased by two orders of magnitude from 2150 to 45 GM, resulting in an almost 50-fold reduction of the brightness. Quantum chemical calculations indicated that the pronounced loss of brightness is primarily a consequence of a strong metal-induced hypsochromic shift of the 2PA maximum from 1.9 to 2.2 eV rather than a loss of two-photon absorptivity across the entire spectral range. Contrary to the large hypsochromic shift of the absorption maximum, the peak emission moved only by 34 nm upon saturation with Mg(II), indicating a weakening of the interaction between the magnesium ion and the aniline nitrogen donor upon photoexcitation. Modified with two symmetrically arranged thioether receptors, the structurally related fluorescent indicator **21** responded with high selectivity towards Ag(I), which promoted efficient fluorescence quenching and a similar metal-induced reduction of the 2PA cross section. The centrosymmetric aminophenol triacetic acid (APTRA) derivative **22** showed an unexpected

bathochromic emission shift upon saturation with Pb(II). Although APTRA was primarily used for the design Mg(II)-selective indicators, the response of **22** proved to be highly selective towards Pb(II) and showed no significant changes in the presence of excess amounts of Mg(II) or Ca(II). Furthermore, a surprisingly small reduction of the 2PA action cross section from 62 to 51 GM was reported.

The presence of two metal-chelating units within the same indicator inevitably leads to solution equilibria composed of multiple coordination species, which make it challenging to deduce metal ion concentrations solely based on the emission response. By replacing one of the metal-binding receptors with a donor moiety that is similar in strength but does not interact with the metal cation, the indicator should largely retain its centrosymmetric electronic structure while eliminating the complications associated with multiple binding sites. For example, the pseudo-centrosymmetric indicator **23** showed indeed a similar 2PA cross section, and saturation with Mg(II) induced again a dramatic reduction from 1800 to 300 GM (λ = 810 nm), resulting in an almost identical action cross section compared to the centrosymmetric parent compound **20**. The closely related compound **24** exhibited qualitatively the same behavior. Saturation with Ca(II) also led to a large decrease of the 2PA cross section from 120 (λ = 760 nm) to 20 GM (λ = 820 nm). In contrast to the Mg(II)-induced spectral changes of **20** and **23**, Ca(II) binding to **24** yielded only a shift in the absorption but not the emission spectrum. The bis(2-pyridyl)amine substituted indicator **25** exhibited strong two-photon induced emission when excited at 780 nm. Upon saturation with Zn(II), the 2PA action cross section was reduced from 14 to 4 GM (λ = 780 nm).

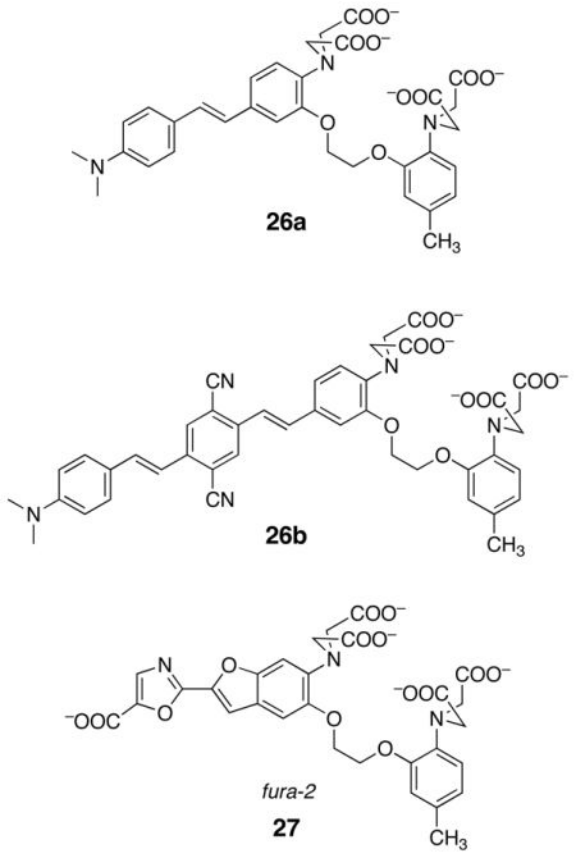

Building upon 1,2-bis(aminophenoxy)ethane-*N,N,N′ N′*-tetraacetic acid (BAPTA), a chelator originally used for the development of the first ratiometric Ca(II) indicator fura-2 (**27**), Dong et al. prepared the probes **26a** and **26b** featuring a pseudocentrosymmetric fluorophore architecture. While **26a** showed only a modest 2PA cross section of 36 GM (λ = 800 nm), extension of the conjugation length improved the maximum absorption to 917 GM (λ = 890 nm) for **26b**. Incubation of HeLa cells with **26b** produced a bright punctate staining pattern as visualized by TPEM; however, upon extracellular stimulation with ATP, the fluorescence emission of **26b** was completely quenched, presumably due to a drastic reduction of the 2PA cross section following a similar mechanism as discussed above for fluorophore **20**. Characterization of fura-2 under two-photon excitation in aqueous buffer solution revealed a 2PA cross section of 12 GM (λ = 700 nm), which was not significantly altered upon saturation with Ca(II)., Although fura-2 features a simple D-π-A architecture, metal binding to the donor moiety similarly reduces the degree of charge transfer upon photoexcitation, which unfavorably impacts the 2PA cross section as discussed above.

While centrosymmetric D-π-A-π-D fluorophores inevitably respond with a reduction of the fluorescence brightness upon binding of metal ions to the terminal donors, emission enhancements can be still achieved when resorting to a different sensing mechanism as recently demonstrated with the calix[4]arene-based indicator **28** (Figure 9). In absence of metal cations, the fluorescence of **28** is presumably quenched through an energy transfer mechanism. Upon binding of K(I) and Pb(II), the indicator emits with a quantum yield of

0.1 and offers a large 2PA cross section of 998 GM (λ = 780 nm). Coordination of K(I) to the crown ether receptor is necessary to achieve the emission enhancement due to an allosteric effect.

Compared to quadrupolar fluorophores, the 2PA cross section of dipolar A-**π**-D structures is typically lower. Nevertheless, the unsymmetrical architecture is better suited for the design of PCT indicators composed of a single chelator moiety, which can be readily attached to the terminal donor or the acceptor sites, thus eliminating the problems associated with multiple binding units. For example, the dipolar indicator **29** is composed of a 1,2,3-triazole-based chelator, which acts both as an electron donor of the PCT fluorophore and as a recognition site for selectively responding towards Zn(II) and Hg(II) ions. In the absence of metal ions, **29** exhibited a maximum 2PA cross section of 350 GM (λ = 820 nm, Table 4), which was lowered to 240 GM (λ = 820 nm) upon saturation with Zn(II). At the same time, the emission maximum was shifted to higher energy, an observation that is consistent with formation of a less polarized excited state due to metal-binding to the terminal donor.

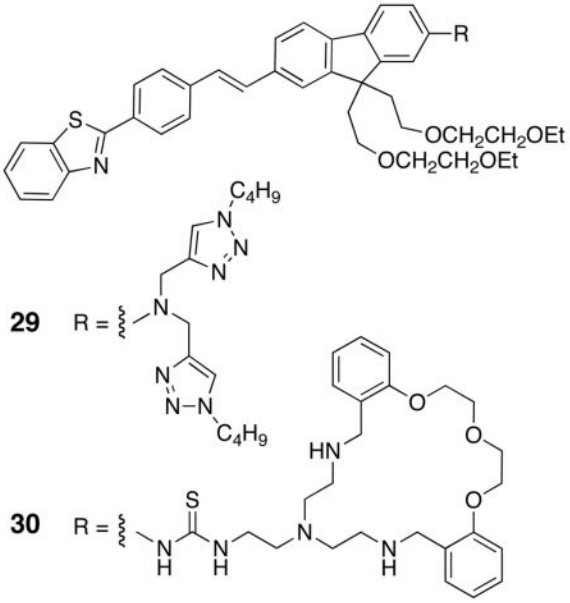

Built upon the same fluorophore platform, indicator **30** displayed a selective response towards Zn(II) ions in THF and water/acetonitrile solution. In the former solvent, the 2PA cross section decreased from 130 to 65 GM (λ = 780 nm) upon Zn(II)-binding (Table 4), whereas in the latter the cross section remained essentially constant around 50 GM (λ = 780 nm). As observed for **29**, the peak emission was blue-shifted by more than 30 nm upon saturation with Zn(II), rendering **30** potentially suitable for ratiometric imaging of Zn(II) in biological systems. Structurally related to the thioether-substituted centrosymmetric indicator **21**, the dipolar structure **31** was designed as Hg(II)-responsive indicator. Maximum 2PA cross sections of 2700 GM and 840 GM (λ = 790 nm) were measured in toluene and in aqueous solution, respectively. Similar to the response of **21** towards Ag(I) ions, saturation of **31** with Hg(II) resulted in complete fluorescence quenching,

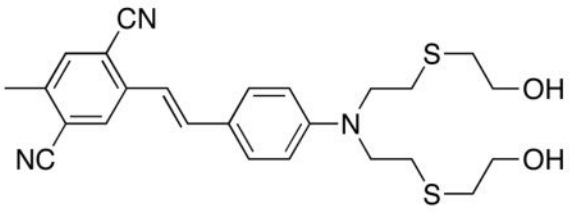

31

All of the above examples utilize the terminal donor moiety as an anchor to integrate a metal-ion recognition site into the fluorophore structure. Because binding of the electropositive metal ion results in reduced donor strength, the 2PA cross section is inevitably lowered, which in turn reduces the brightness of the fluorescence emission. For biological TPEM imaging, however, it would be desirable to generate an increase rather than decrease in fluorescence contrast upon metal binding. This can be achieved with an alternate fluorophore design, in which the metal ion binds to the acceptor rather than donor moiety of the dipolar A-**π**–D scaffold. In this case, the excited state polarization is increasing upon metal binding, which should also yield an increased 2PA cross section according to equation 4. Most electron accepting groups traditionally used in dipolar fluorophores are poor Lewis bases and therefore not suitable for metal ion coordination; however, pyridine forms a wide range of coordination complexes and can act as an effective **π**-acceptor with similar strength compared to carboxylic acid esters. For example, the Zn(II)-responsive indicator **32** was designed following this approach. The molecule is composed of a electron-donating anisole substituent, which is linked to the electron-deficient tris(picolyl)amine Zn(II) receptor through an oxazole bridge. Upon saturation with Zn(II), the 2PA cross section increased from 31 (λ = 690 nm) to 77 GM (λ = 730 nm) and the emission maximum shifted from 441 to 497 nm, a significant spectral change suitable for ratiometric measurements. Contrary to fluorophores with a centrosymmetric D-**π**-A-**π**–D architecture, the fluorescence brightness increased rather than decreased upon Zn(II) binding. At wavelengths above 800 nm, the 2PA cross section is vanishingly small for the metal-free indicator but strongly enhanced upon Zn(II) binding, thus producing a very large fluorescence contrast of greater than 1:10,000.

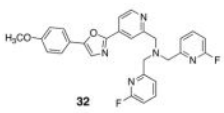

32

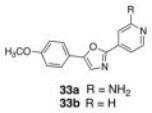

33a R = NH_2
33b R = H

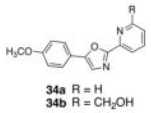

34a R = H
34b R = CH_2OH

The structurally related compounds **33** and **34** were designed as probes for ratiometric pH measurements in aqueous solution., Protonation of the pyridine moiety significantly increases the acceptor strength, which in turn leads to a strongly red-shifted fluorescence emission and an increased 2PA cross section. For example, under neutral conditions the amino-substituted derivative **33a** exhibited a maximum 2PA cross section of 15 GM (λ = 710 nm), which increased to 65 GM (λ = 800 nm) upon acidification to pH 2. At the same time, fluorescence emission was shifted from 465 to 530 nm upon protonation. Depending on the substituent in the 2-position, the pyrdine pK_a can be adjusted over a wide range while maintaining the enhanced two-photon response. For example, derivative **33b** lacking the hydrazine substituent has a pK_a of 4.3, which is even further lowered to 2.6 and 1.8 in the ortho-substituted derivatives **34a** and **34b**, respectively.

The Mg(II)-selective indicator **35** is derived from the dipolar benzo[h]chromene label **4a** discussed in section 2.2.1. The caboxylate group and neighboring carbonyl oxygen form a bidentate ligand, which functions also as an effective π-acceptor. Consistent with an increased excited state polarization upon binding with Mg(II), the maximum 2PA cross section was shifted to lower energy and increased from 290 (λ = 820 nm) to 382 GM (λ = 880 nm). With a binding affinity of 2.5 mM, the indicator was well suited for detecting Mg(II) ions in live cells and mouse hippocampal tissue (Figure 10).

Featuring an octupolar architecure with three D-π-A branches, chromophore **36** showed also a strong Zn(II)-induced increase of the 2PA cross section. The increased excited state polarization of the Zn(II)-bound form was again responsible for a strongly red-shifted emission spectrum compared to the unbound fluorophore.

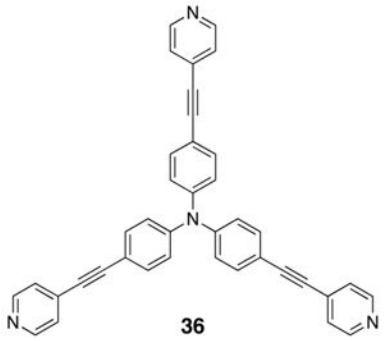

36

2.3.2. Photoinduced Electron Transfer Probes (PET)—As discussed in the previous section, photoexcitation of dipolar and quadrupolar molecules is associated with a large charge redistribution in the excited state. In addition, the open-shell electron configuration of the excited fluorophore is responsible for fundamentally altered redox properties. Compared to the ground state, the photo-excited state is both a better oxidant and reductant, a property that can be harnessed to modulate the fluorescence output in an analyte dependent manner through an electron transfer reaction. For this purpose, the metal-ion receptor must be electronically decoupled from the fluorophore π-system, otherwise photoexcitation would lead to formation of a simple charge transfer state as previously discussed. Hence, upon photoexcitation an electron transfer reaction can occur between the metal-ion receptor acting as the donor (D), and the excited fluorophore (F*) acting as the acceptor (Figure 11a). Because charge recombination of the intermediately formed radical ion pair ($D^{\bullet+}$–$F^{\bullet-}$) is typically a non-radiative process, photoinduced electron transfer (PET) usually results in quenching of the fluorescence emission. Metal coordination to the receptor is expected to render the PET process less favorably, which in turn leads to an emission increase (Figure 11b). Because the quenching electron donor is electronically decoupled form the fluorophore, this design strategy has the advantage that the 2PA cross section and emission energy are not significantly affected by metal binding.

Based on this approach, Cho and coworkers have developed a broad range of fluorescent two-photon indicators that respond with an emission increase upon binding of the respective analyte (Figure 12).

In all of these indicators a donor-acceptor substituted dipolar naphthalene scaffold serves as two-photon absorbing fluorophore, which was combined in a modular fashion with a wide range of receptors acting as PET donors. Depending on the nature of the sensing moiety, the two-photon action cross section of derivatives **37–43** ranged between 86 and 125 GM (λ = 780 nm) (Table 5). For example, fluorophores **37** and **38** were designed as pH responsive probes. The aniline moiety in **37a** has a sufficiently low redox potential to quench the fluorescence emission through a PET mechanism. Upon protonation at low pH, the aniline donor is rendered electrochemically inactive and no longer quenches the emission of the naphthalene fluorophore, thus resulting in a 22-fold fluorescence emission increase. Substitution with a methoxy group further decreased the redox potential of the aniline donor, which resulted in more effective quenching and a 3-fold improved fluorescence enhancement factor of 64 for derivative **37b**. The probe was successfully applied to visualize acidic compartments in macrophages using TPEM. The redox potential of the aliphatic amino group of **38** is too high for engaging in PET quenching; however, the probe is effectively trapped upon protonation in acidic compartments and was successfully used to label acidic vesicles, live macrophages and acute rat hippocampal slices. Given the favorable redox potential of BAPTA, the fluorescence of indicator **39** is also effectively quenched through a PET mechanism. The probe selectively responds to Ca(II) over other divalent metal ions and has been used to visualize calcium waves in astrocytes and acute rat hypothalamic slices. Similarly, the APTRA-functionalized indicator **41** exhibited a 15-fold fluorescence increase upon saturation with Mg(II) ions. The probe was readily loaded into live Hep3B cells and acute mouse hippocampal slices. With a dissociation constant of K_d = 2.5 mM the indicator was suitable for dynamically imaging changes in cellular Mg(II) concentrations. Hydrophobic fluorescent probes such as **38** and **41** tend to partition into cellular membranes. Because the encountered low polarity environment destabilizes the radical ion pair formed as an intermediate in the PET quenching process, the fluorescence quantum yield of hydrophobic PET indicators may increase simply due to membrane partitioning rather than analyte binding. This problem has been elegantly addressed by taking advantage of the polarity dependent emission spectrum of the dipolar naphthalene fluorophore. Live cell imaging studies revealed a blue-shifted emission maximum for the membrane-localized probes **38** and **41** compared to the charged metal-bound forms, which preferentially localized in the cytosolic environment. The artifact free detection of cellular Ca(II) and Mg(II) was readily accomplished by collecting only the lower-energy portion of the fluorescence emission, corresponding to the metal-ion dependent response of the cytosolically localized probe., Utilizing the environmental sensitive probe laurdan as fluorescent core, the indicators **44a** and **44b** were specifically designed for imaging Ca(II) fluxes near membranes in live cells., Compared to calcium green and fura-2, which were developed for linear microscopy, the indicators are 3-times brighter with two-photon excitation.

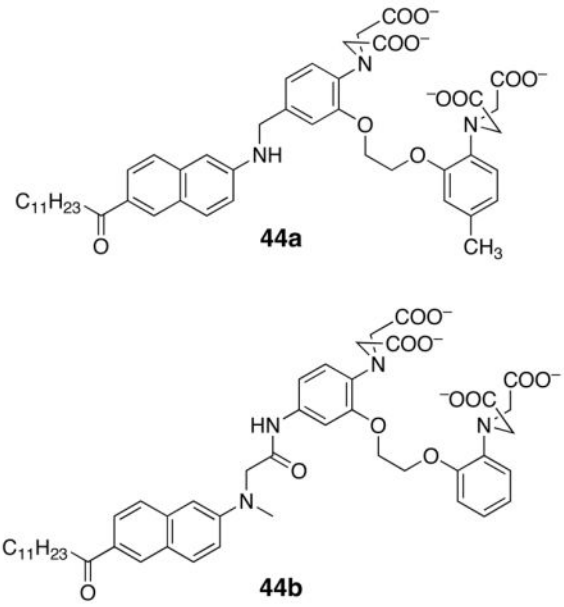

The fluorescent indicator **40** responded with a 8-fold fluorescence enhancement upon saturation with sodium ions and was successfully utilized for imaging glutamate induced changes of intracellular Na(I) concentrations in astrocytes. Treatment with ouabain, a steroid hormone that inhibits Na^+/K^+ ATPases, led also to a dramatic increase of cytosolic Na(I). The selective detection of Zn(II) ions was accomplished with indicator **42a** and **42b** which contain *N,N*-di(2-picolyl)ethylenediamine (DPEN) as receptor moiety. As already discussed for the pH-sensitive indicators **37a** and **37b**, substitution with a methoxy group in **42b** yielded more efficient quenching in absence of metal ions and a further improved fluorescence enhancement upon saturation with Zn(II). Indicator **42b** proved to be useful for imaging labile Zn(II) stores in acute rat hippocampal slices as well as monitoring the release of endogenous Zn(II) pools upon stimulation of 293 cells with 10 mM *S*-nitrosocysteine. Despite the rather low fluorescence contrast, indicator **43** was successfully used for the quantification of Hg(II) ions in kidney, heart, liver, and gill tissue of *oryzias latipes* after exposure to 2 ppb Hg(II) for 1–3 days.

2.3.3. Excited State Proton Transfer Probes—In some fluorophores, the electron redistribution in the photo-excited state leads to dramatic changes in the acidity or basicity of heteroatom substituents., For example, the acidity of 2-naphthol increases from $pK_a = 9.5$ in the ground state to $pK_a^* = 2.8$ in the lowest excited singlet state. This change is sufficient to initiate a proton transfer to a nearby water molecule within the radiative lifetime of the excited state, thus giving rise to fluorescence emission from the deprotonated 2-naphtholate anion. Fluorophores in which the photo-acidic group is combined with a suitable proton acceptor may also undergo an excited state intramolecular proton transfer (ESIPT) reaction. By integrating the proton acceptor or donor moiety into a metal-ion chelator, the ESIPT process can be disrupted in a metal ion-dependent fashion to produce a change in fluorescence output (Figure 13).

For example, benzazole substituted phenols **45** undergo an excited state intramolecular proton transfer (ESIPT) to yield the corresponding phototautomer T* as illustrated with the Jablonski diagram in Figure 13a. The proton transfer reaction usually occurs at such a fast rate that no fluorescence emission from the normal tautomer N* is observed. After radiative deactivation, the phototautomer thermally equilibrates back to its initial ground state. Upon coordination of a metal ion to benzazole scaffold, ESIPT is inhibited and the fluorescence emission now occurs at substantially higher energy (Figure 13b). In view of the large change in emission energy, this switching mechanism is particularly attractive for the design of emission ratiometric indicators.

Figure 14 shows a few selected examples of fluorophores which utilize an ESIPT switching mechanism to produce a chromatic shift of the fluorescence upon Zn(II) coordination. Beside the expected photo-tautomer emission, 2-(2′-hydroxyphenyl)-benzimidazole derivative **46** produced also a higher energy band that was assigned to the presence of ground state rotamers. After replacing the hydroxy group with an arylsulfonamide as hydrogen bond donor, the formation of rotamers was effectively abolished. Photoexcitation of **47** produced a single, strongly Stokes shifted emission band, which moved to higher energy upon saturation with Zn^{2+}. By changing the denticity of the coordination site, the binding affinity of **47** was readily tuned without significantly altering the photophysical properties. While the Zn(II)-responsive indicators **46** and **47** were not evaluated in a biological setting, the structurally related probe **48** (Zinbo-5) proved to be suitable for detecting changes of intracellular Zn(II) pools by emission ratiometric TPEM (Figure 15).

The centrosymmetric benzazole derivative **49** exhibited a 2PA cross section of 530 GM (λ = 740 nm) in DMF which slightly decreased to 470 GM (λ = 740 nm) upon saturation with Zn(II). In the absence of metal ions, the indicator showed a low-energy emission band of the phototautomer; however, presumably due to the presence of ground state rotamers, an additional band at higher energy appeared. Coordination of Zn(II) yielded a uniform emission band at higher energy relative to the tautomer fluorescence. Under basic conditions, a very large cross section of 4120 GM was found for the bisphenolate dianionic species. The bis(2-picolyl)amine-modified quinoline derivative **50** is presumably also engaged in an excited state proton transfer process, in which the quinoline nitrogen is protonated. Contrary to the benzazole fluorophores discussed above, the photoproduct is non-fluorescent and thus the emission of **50** is effectively quenched. Upon saturation with Zn(II), a 14-fold emission enhancement was observed. The indicator was tested in A431 cells by TPEM and showed a strong emission response upon incubation with exogenous Zn(II).

3. Fluorescent Labels and Indicators Commonly Used in Biological Research

Despite the many well-established and proven design strategies, the 2PA action cross sections achieved in polar solvents, and more specifically, in aqueous buffer solution at high ionic strength, are modest and typically do not exceed 200 GM as apparent from the preceding sections. Although most of the fluorescent indicators and labels that are

commonly used in biological research offer only small 2PA cross sections, their sensitivity may be still sufficient for routine TPEM imaging applications. Given that most of these dyes are readily available, either as bioconjugatable labels or already attached to antibodies, peptides, lipids, or drugs, their application in TPEM remains an attractive alternative. For this reason, we conclude this review with a brief overview of the 2PA cross sections and photophysical properties of commonly used biological labels and probes that were not specifically developed for TPEM (Table 6).

With a cross section of 180 GM, rhodamine B ranks among the brightest of the traditional fluorescent labels. Because fura-2 does not exhibit significant changes in the emission spectrum upon Ca(II)-binding, this indicator is not suitable for ratiometric TPEM imaging; nevertheless, after careful calibration the dye has been successfully applied to dynamically image intracellular Ca(II) by TPEM within the mammalian cerebral cortex, an epithelial cell line, and in ventricular cardiomyocytes. In contrast, indo-1 undergoes a Ca(II)-induced shift of the peak emission, rendering this dye well suited for ratiometric TPEM. For example, indo-1 was used to visualize voltage induced intracellular Ca(II) waves in fish keratocytes and Ca(II) transients in the course of the mouse sperm-egg fusion.

Mostly based on established fluorophore platforms, numerous cation sensors for the detection of other biologically important metal ions have been developed. Although their photophysical properties were not optimized for two-photon excitation, many of the probes have been successfully employed in TPEM. For example, intracellular zinc stores were visualized in cell culture and in mossy fiber synapses of live hippocampal slices by TPEM with fluorescein-based probes., Zinquin, one of the early zinc-selective fluorescent probes was utilized for imaging zinc-rich intracellular compartments in primary cultured hippocampal neurons.

A number of biomolecules such as NAD(P)H or flavoproteins are intrinsically fluorescent and can be directly visualized by TPEM., While their cross section is significantly smaller compared to exogenous fluorescent labels (Table 6), TPEM of biomolecules offers the opportunity to non-invasively study biological processes under physiological conditions. Taking advantage of its fluorescent properties, the in vivo distribution of NAD(P)H has been visualized in human skin cells as well as in mitochondria of skeletal muscles., Finally, green fluorescent protein (GFP) and its variants exhibit also substantial 2PA cross sections and offer particularly exciting possibilities to label and track proteins in live cells.,

4. Conclusions

Over the past decade, TPEM has rapidly emerged as a valuable technique in the toolbox of the cell biologist. By exploiting a diverse array of rational design strategies, a substantial number of fluorescent probes and labels with optimized 2PA properties have been developed. Compared to traditional probes and labels, the 2PA cross sections have been improved by approximately one order of magnitude with the benefit of enhancing their optical sensitivity and thus allowing excitation at lower laser power. While the development of organic fluorophores with further improved 2PA cross section remains an important goal, the boundaries imposed by the spectral window of the Ti-sapphire laser used as excitation

source in TPEM combined with the polar aqueous environment encountered in biological studies appear to set a limit to the maximum achievable 2PA action cross section and optical sensitivity. For example, while organic fluorophores with centrosymmetric architecture offer high 2PA cross sections in organic solvent, their highly polarized excited states give rise to increased non-radiative deactivation in an aqueous environment and thus substantially diminished quantum yields. Furthermore, the lowest energy two-photon allowed state in centrosymmetric fluorophores is S_2, whereas according to Kasha's rule emission occurs from S_1 at lower energy, which might be insufficient to drive a PET process necessary for cation-induced fluorescence switching. Finally, the integration of a single cation-binding site into a centrosymmetric architecture poses additional challenges. Although the latter problem can be addressed with architectures containing two cation-binding sites, an unbalanced occupancy inevitably results in symmetry breaking, which in turn jeopardizes the 2PA cross section. The presence of multiple coordination species with different photophysical properties renders the quantitative interpretation of the emission response particularly challenging. For these reasons, non-centrosymmetric fluorophores appear to be better suited for the design of robust cation-responsive probes; however, their cross sections in the 700–950 nm range rarely exceed 100 GM. Regardless of their molecular symmetry, the majority of fluorophores with optimized 2PA are based on extended linear π-systems, thus imposing a high degree of lipophilicity that must be counterbalanced with charged or polar hydrophilic substituents. At present, membrane permeant TPEM probes tend to partition within lipid bilayers of intracellular compartments and organelles and offer little control over their subcellular distribution. The accumulation in specific compartment deserves particular attention, since the distribution of endogenous metal pools could be directly influenced by a probe acting as an ionophore. Furthermore, the lower polarity environment of cellular membranes may affect the fluorescence response of the probe in a metal-independent manner and thus yield undesired artifacts. These challenges could be in part addressed by the recently developed bio-orthogonal labeling approaches such as the SNAP tag– or HaloTag, where the probe or label is covalently tethered to a well-defined protein pocket that would protect from environment-dependent influences. While the majority of work has focused on optimizing the 2PA cross section of organic materials, semiconductor quantum dots and coinage metal nanoclusters have been reported to be robust emitters with extraordinary large 2PA cross sections,– thus potentially leading the way towards alternative strategies for the design of ultrabright and highly sensitive cation-responsive probes for biological TPEM imaging.

Acknowledgments

Financial support from the National Institutes of Health (R01DK68096) is gratefully acknowledged.

References

1. Waldron KJ, Rutherford JC, Ford D, Robinson NJ. Metalloproteins and metal sensing. Nature. 2009; 460(7257):823–830. [PubMed: 19675642]
2. McRae R, Bagchi P, Sumalekshmy S, Fahrni CJ. In situ imaging of metals in cells and tissues. Chem Rev. 2009; 109(10):4780–4827. [PubMed: 19772288]
3. Lord SJ, Lee HLD, Moerner WE. Single-molecule spectroscopy and imaging of biomolecules in living cells. Anal Chem. 2010; 82(6):2192–2203. [PubMed: 20163145]

4. Grynkiewicz G, Poenie M, Tsien RY. A new generation of Ca(II) indicators with greatly improved fluorescence properties. J Biol Chem. 1985; 260(6):3440–3450. [PubMed: 3838314]
5. de Silva AP, Gunaratne HQN, Gunnlaugsson T, Huxley AJM, McCoy CP, Rademacher JT, Rice TE. Signaling recognition events with fluorescent sensors and switches. Chem Rev. 1997; 97(5):1515–1566. [PubMed: 11851458]
6. Domaille DW, Que EL, Chang CJ. Synthetic fluorescent sensors for studying the cell biology of metals. Nat Chem Biol. 2008; 4(3):168–175. [PubMed: 18277978]
7. Diaspro A, Chirico G, Collini M. Two-photon fluorescence excitation and related techniques in biological microscopy. Q Rev Biophys. 2005; 38(2):97–166. [PubMed: 16478566]
8. Helmchen F, Denk W. Deep tissue two-photon microscopy. Nat Methods. 2005; 2(12):932–940. [PubMed: 16299478]
9. Kerr JND, Denk W. Imaging in vivo: watching the brain in action. Nat Rev Neurosci. 2008; 9(3): 195–205. [PubMed: 18270513]
10. Niggli E, Egger M. Applications of multi-photon microscopy in cell physiology. Frontiers in Bioscience. 2004; 9:1598–1610. [PubMed: 14977571]
11. So PTC, Dong CY, Masters BR, Berland KM. Two-photon excitation fluorescence microscopy. Annual Review of Biomedical Engineering. 2000; 2:399–429.
12. Zipfel WR, Williams RM, Webb WW. Nonlinear magic: multiphoton microscopy in the biosciences. Nat Biotechnol. 2003; 21(11):1368–1376.
13. Denk W, Strickler JH, Webb WW. 2-Photon laser scanning fluorescence microscopy. Science. 1990; 248(4951):73–76. [PubMed: 2321027]
14. Albota M, Beljonne D, Brédas J-L, Ehrlich JE, Fu JY, Heikal AA, Hess SE, Kogej T, Levin MD, Marder SR, McCord-Maughon D, Perry JW, Rockel H, Rumi M, Subramaniam C, Webb WW, Wu XL, Xu C. Design of organic molecules with large two-photon absorption cross sections. Science. 1998; 281(5383):1653–1656. [PubMed: 9733507]
15. Kogej T, Beljonne D, Meyers F, Perry JW, Marder SR, Brédas J-L. Mechanisms for enhancement of two-photon absorption in donor-acceptor conjugated chromophores. Chem Phys Lett. 1998; 298(1–3):1–6.
16. Reinhardt BA, Brott LL, Clarson SJ, Dillard AG, Bhatt JC, Kannan R, Yuan LX, He GS, Prasad PN. Highly active two-photon dyes: Design, synthesis, and characterization toward application. Chem Mat. 1998; 10(7):1863–1874.
17. Barzoukas M, Blanchard-Desce M. Molecular engineering of push-pull dipolar and quadrupolar molecules for two-photon absorption: A multivalence-bond states approach. J Chem Phys. 2000; 113(10):3951–3959.
18. Rumi M, Ehrlich JE, Heikal AA, Perry JW, Barlow S, Hu ZY, McCord-Maughon D, Parker TC, Rockel H, Thayumanavan S, Marder SR, Beljonne D, Brédas J-L. Structure-property relationships for two-photon absorbing chromophores: Bis-donor diphenylpolyene and bis(styryl)benzene derivatives. J Am Chem Soc. 2000; 122(39):9500–9510.
19. Strehmel, B., Strehmel, V. Two-photon physical, organic, and polymer chemistry: theory, techniques, chromophore design, and applications. In: Neckers, DC.Jenks, WS., Wolff, T., editors. Advances in Photochemistry. Wiley; 2006. p. 111-354.
20. Terenziani F, Katan C, Badaeva E, Tretiak S, Blanchard-Desce M. Enhanced two-photon absorption of organic chromophores: theoretical and experimental assessments. Adv Mater. 2008; 20(24):4641–4678.
21. Rumi M, Barlow S, Wang J, Perry JW, Marder SR. Two-photon absorbing materials and two-photon-induced chemistry. Adv Polym Sci. 2008; 213:1–95.
22. He GS, Tan LS, Zheng Q, Prasad PN. Multiphoton absorbing materials: Molecular designs, characterizations, and applications. Chem Rev. 2008; 108(4):1245–1330. [PubMed: 18361528]
23. Kim HM, Cho BR. Two-photon materials with large two-photon cross sections. Structure-property relationship. Chem Commun. 2009; 2:153–164.
24. Pawlicki M, Collins HA, Denning RG, Anderson HL. Two-photon absorption and the design of two-photon dyes. Angew Chem Int Ed Engl. 2009; 48(18):3244–3266. [PubMed: 19370705]
25. Göppert-Mayer M. Über Elementarakte mit zwei Quantensprüngen. Ann Phys (Leipzig). 1931; 5:273–294.

26. Schafer-Hales KJ, Belfield KD, Yao S, Frederiksen PK, Hales JM, Kolattukudy PE. Fluorene-based fluorescent probes with high two-photon action cross-sections for biological multiphoton imaging applications. J Biomed Opt. 2005; 10(5):015402.
27. Andrade CD, Yanez CO, Rodriguez L, Belfield KD. A series of fluorene-based two-photon absorbing molecules: synthesis, linear and nonlinear characterization, and bioimaging. J Org Chem. 2010; 75(12):3975–3982. [PubMed: 20481596]
28. Barsu C, Cheaib R, Chambert S, Queneau Y, Maury O, Cottet D, Wege H, Douady J, Bretonniere Y, Andraud C. Neutral push-pull chromophores for nonlinear optical imaging of cell membranes. Org Biomol Chem. 2010; 8(1):142–150. [PubMed: 20024145]
29. Barsu C, Fortrie R, Nowika K, Baldeck PL, Vial J-C, Barsella A, Fort A, Hissler M, Bretonnière Y, Maury O, Andraud C. Synthesis of chromophores combining second harmonic generation and two photon induced fluorescence properties. Chem Commun. 2006; (45):4744–4746.
30. Kim HM, Fang XZ, Yang PR, Yi JS, Ko YG, Piao MJ, Chung YD, Park YW, Jeon SJ, Cho BR. Design of molecular two-photon probes for in vivo imaging. 2H-benzo[h]chromene-2-one derivatives. Tetrahedron Lett. 2007; 48(15):2791–2795.
31. Gallagher SS, Jing CR, Peterka DS, Konate M, Wombacher R, Kaufman LJ, Yuste R, Cornish VW. A trimethoprim-based chemical tag for live cell two-photon imaging. ChemBioChem. 2010; 11(6): 782–784. [PubMed: 20217883]
32. Chui C-H, Wang Q, Chow W-C, Yuen MC-W, Wong K-L, Kwok W-M, Cheng GY-M, Wong RS-M, Tong S-W, Chan K-W, Lau F-Y, Lai PB-S, Lam K-H, Fabbri E, Tao X-M, Gambari R, Wong W-Y. 5-(Dimethylamino)-N-(4-ethynylphenyl)-1-naphthalenesulfonamide as a novel bifunctional antitumor agent and two-photon induced bio-imaging probe. Chem Commun. 2010; 46(20):3538–3540.
33. Albota MA, Xu C, Webb WW. Two-photon fluorescence excitation cross sections of biomolecular probes from 690 to 960 nm. Appl Opt. 1998; 37(31):7352–7356. [PubMed: 18301569]
34. Hayek A, Bolze F, Nicoud JF, Baldeck PL, Mély Y. Synthesis and characterization of water-soluble two-photon excited blue fluorescent chromophores for bioimaging. Photochem Photobiol Sci. 2006; 5(1):102–106. [PubMed: 16395434]
35. Hayek A, Grichine A, Huault T, Ricard C, Bolze F, van der Sanden B, Vial JC, Mély Y, Duperray A, Baldeck PL, Nicoud JF. Cell-permeant cytoplasmic blue fluorophores optimized for in vivo two-photon microscopy with low-power excitation. Microsc Res Techn. 2007; 70(10):880–885.
36. Hayek A, Bolze F, Bourgogne C, Baldeck PL, Didier P, Arntz Y, Mély Y, Nicoud JF. Boron containing two-photon absorbing chromophores. 2. Fine tuning of the one- and two-photon photophysical properties of pyrazabole based fluorescent bioprobes. Inorg Chem. 2009; 48(19): 9112–9119. [PubMed: 19728694]
37. Hawthorne MF. The role of chemistry in the development of boron neutron-capture therapy of cancer. Angew Chem Int Ed Engl. 1993; 32(7):950–984.
38. Morales AR, Luchita G, Yanez CO, Bondar MV, Przhonska OV, Belfield KD. Linear and nonlinear photophysics and bioimaging of an integrin-targeting water-soluble fluorenyl probe. Org Biomol Chem. 2010; 8(11):2600–2608. [PubMed: 20376401]
39. Woo HY, Liu B, Kohler B, Korystov D, Mikhailovsky A, Bazan GC. Solvent effects on the two-photon absorption of distyrylbenzene chromophores. J Am Chem Soc. 2005; 127(42):14721–14729. [PubMed: 16231926]
40. Woo HY, Hong JW, Liu B, Mikhailovsky A, Korystov D, Bazan GC. Water-soluble [2.2]paracyclophane chromophores with large two-photon action cross sections. J Am Chem Soc. 2005; 127(3):820–821. [PubMed: 15656604]
41. Das S, Nag A, Goswami D, Bharadwaj PK. Zinc(II)- and copper(I)-mediated large two-photon absorption cross sections in a bis-cinnamaldiminato Schiff base. J Am Chem Soc. 2006; 128(2): 402–403. [PubMed: 16402814]
42. Kamada K, Matsunaga K, Yoshino A, Ohta K. Two-photon-absorption-induced accumulated thermal effect on femtosecond Z-scan experiments studied with time-resolved thermal-lens spectrometry and its simulation. J Opt Soc Am B - Opt Phys. 2003; 20(3):529–537.

43. Zhang X-B, Feng J-K, Ren A-M. Theoretical study of the two-photon absorption properties of octupolar complexes with Cu(I), Zn(II) and Al(III) as centers and bis-cinnamaldimine as ligands. J Organomet Chem. 2007; 692(17):3778–3787.
44. Mazzucato S, Fortunati I, Scolaro S, Zerbetto M, Ferrante C, Signorini R, Pedron D, Bozio R, Locatelli D, Righetto S, Roberto D, Ugo R, Abbotto A, Archetti G, Beverina L, Ghezzi S. Two-photon absorption of Zn(II) octupolar molecules. Phys Chem Chem Phys. 2007; 9(23):2999–3005. [PubMed: 17551624]
45. Feuvrie C, Maury O, Le Bozec H, Ledoux I, Morrall JP, Dalton GT, Samoc M, Humphrey MG. Nonlinear optical and two-photon absorption properties of octupolar tris(bipyridyl)metal complexes. J Phys Chem A. 2007; 111(37):8980–8985. [PubMed: 17722893]
46. Dragonetti C, Balordi M, Colombo A, Roberto D, Ugo R, Fortunati I, Garbin E, Ferrante C, Bozio R, Abbotto A, Le Bozec H. Two-photon absorption properties of Zn(II) complexes: Unexpected large TPA cross section of dipolar [ZnY_2(4,4′-bis(para-di-n-butylaminostyryl)-2,2′-bipyridine)] (Y = Cl, CF_3CO_2). Chem Phys Lett. 2009; 475(4–6):245–249.
47. Ray D, Nag A, Goswami D, Bharadwaj PK. Acyclic donor-acceptor-donor chromophores for large enhancement of two-photon absorption cross-section in the presence of Mg(II), Ca(II) or Zn(II) ions. J Lumin. 2009; 129(3):256–262.
48. Andraud C, Maury O. Lanthanide complexes for nonlinear optics: From fundamental aspects to applications. Eur J Inorg Chem. 2009; (29–30):4357–4371.
49. D'Aléo A, Pompidor G, Elena B, Vicat J, Baldeck PL, Toupet L, Kahn R, Andraud C, Maury O. Two-photon microscopy and spectroscopy of lanthanide bioprobes. Chem Phys Chem. 2007; 8(14):2125–2132. [PubMed: 17847141]
50. Picot A, D'Aléo A, Baldeck PL, Grichine A, Duperray A, Andraud C, Maury O. Long-lived two-photon excited luminescence of water-soluble europium complex: applications in biological imaging using two-photon scanning microscopy. J Am Chem Soc. 2008; 130(5):1532–1533. [PubMed: 18193870]
51. Pond SJK, Tsutsumi O, Rumi M, Kwon O, Zojer E, Brédas J-L, Marder SR, Perry JW. Metal-ion sensing fluorophores with large two-photon absorption cross sections: aza-crown ether substituted donor-acceptor-donor distyrylbenzenes. J Am Chem Soc. 2004; 126(30):9291–9306. [PubMed: 15281820]
52. Huang CB, Peng XJ, Lin ZY, Fan JL, Ren AX, Sun DX. A highly selective and sensitive two-photon chemosensor for silver ion derived from 3,9-dithia-6-azaundecane. Sens Actuators B. 2008; 133(1):113–117.
53. Cui JQ, Fan JL, Peng XJ, Sun SG, Chen GC, Guo KX. A new fluorescent sensor selective for Pb(II) in water capable of two-photon-induced fluorescence measurement. Sci China, Ser B. 2009; 52(6):780–785.
54. Kim HM, Jeong M-Y, Ahn HC, Jeon S-J, Cho BR. Two-photon sensor for metal ions derived from azacrown ether. J Org Chem. 2004; 69(17):5749–5751. [PubMed: 15307750]
55. Ahn HC, Yang SK, Kim HM, Li SJ, Jeon S-J, Cho BR. Molecular two-photon sensor for metal ions derived from bis(2-pyridyl)amine. Chem Phys Lett. 2005; 410(4–6):312–315.
56. Dong XH, Yang YY, Sun J, Liu ZH, Liu B-F. Two-photon excited fluorescent probes for calcium based on internal charge transfer. Chem Commun. 2009; (26):3883–3885.
57. Xu C, Zipfel W, Shear JB, Williams RM, Webb WW. Multiphoton fluorescence excitation: New spectral windows for biological nonlinear microscopy. Proc Natl Acad Sci USA. 1996; 93(20): 10763–10768. [PubMed: 8855254]
58. Wokosin DL, Loughrey CM, Smith GL. Characterization of a range of fura dyes with two-photon excitation. Biophys J. 2004; 86(3):1726–1738. [PubMed: 14990500]
59. Kim JS, Kim HJ, Kim HM, Kim SH, Lee JW, Kim SK, Cho BR. Metal ion sensing novel calix[4]crown fluoroionophore with a two-photon absorption property. J Org Chem. 2006; 71(21): 8016–8022. [PubMed: 17025289]
60. Nguyen DM, Frazer A, Rodriguez L, Belfield KD. Selective fluorescence sensing of zinc and mercury ions with hydrophilic 1,2,3-triazolyl fluorene probes. Chem Mat. 2010; 22(11):3472–3481.

61. Belfield KD, Bondar MV, Frazer A, Morales AR, Kachkovsky OD, Mikhailov IA, Masunov AE, Przhonska OV. Fluorene-Based Metal-Ion Sensing Probe with High Sensitivity to Zn(II) and Efficient Two-Photon Absorption. J Phys Chem B. 2010; 114(28):9313–9321. [PubMed: 20590077]
62. Huang CB, Fan JL, Peng XJ, Lin ZY, Guo BP, Ren AX, Cui JQ, Sun SG. Highly selective and sensitive twin-cyano-stilbene-based two-photon fluorescent probe for mercury(II) in aqueous solution with large two-photon absorption cross-section. J Photochem Photobiol. 2008; 199(2–3): 144–149.
63. Sumalekshmy S, Henary MM, Siegel N, Lawson PV, Wu Y, Schmidt K, Brédas J-L, Perry JW, Fahrni CJ. Design of emission ratiometric metal-ion sensors with enhanced two-photon cross section and brightness. J Am Chem Soc. 2007; 129(39):11888–11889. [PubMed: 17845038]
64. Charier S, Ruel O, Baudin J-B, Alcor D, Allemand JF, Meglio A, Jullien L. An efficient fluorescent probe for ratiometric pH measurements in aqueous solutions. Angew Chem Int Ed Engl. 2004; 43(36):4785–4788. [PubMed: 15366087]
65. Charier S, Ruel O, Baudin J-B, Alcor D, Allemand J-F, Meglio A, Jullien L, Valeur B. Photophysics of a series of efficient fluorescent pH probes for dual-emission-wavelength measurements in aqueous solutions. Chem Eur J. 2006; 12(4):1097–1113. [PubMed: 16247827]
66. Kim HM, Yang PR, Seo MS, Yi J-S, Hong JH, Jeon S-J, Ko Y-G, Lee KJ, Cho BR. Magnesium ion selective two-photon fluorescent probe based on a benzo[*h*]chromene derivative for in vivo imaging. J Org Chem. 2007; 72(6):2088–2096. [PubMed: 17316048]
67. Bhaskar A, Ramakrishna G, Twieg RJ, Goodson T. Zinc sensing via enhancement of two-photon excited fluorescence. J Phys Chem C. 2007; 111(40):14607–14611.
68. Kim HM, Cho BR. Two-photon probes for intracellular free metal ions, acidic vesicles, and lipid rafts in live tissues. Acc Chem Res. 2009; 42(7):863–872. [PubMed: 19334716]
69. Kim HM, An MJ, Hong JH, Jeong BH, Kwon O, Hyon JY, Hong SC, Lee KJ, Cho BR. Two-photon fluorescent probes for acidic vesicles in live cells and tissue. Angew Chem Int Ed Engl. 2008; 47(12):2231–2234. [PubMed: 18273843]
70. Kim HM, Kim BR, Hong JH, Park JS, Lee KJ, Cho BR. A two-photon fluorescent probe for calcium waves in living tissue. Angew Chem Int Ed Engl. 2007; 46(39):7445–7448. [PubMed: 17680568]
71. Kim HM, Jung C, Kim BR, Jung SY, Hong JH, Ko YG, Lee KJ, Cho BR. Environment-sensitive two-photon probe for intracellular free magnesium ions in live tissue. Angew Chem Int Ed Engl. 2007; 46(19):3460–3463. [PubMed: 17397120]
72. Parasassi T, De Stasio G, d'Ubaldo A, Gratton E. Phase fluctuation in phospholipid membranes revealed by Laurdan fluorescence. Biophys J. 1990; 57(6):1179–1186. [PubMed: 2393703]
73. Mohan PS, Lim CS, Tian YS, Roh WY, Lee JH, Cho BR. A two-photon fluorescent probe for near-membrane calcium ions in live cells and tissues. Chem Commun. 2009; (36):5365–5367.
74. Shin YN, Lim CS, Tian YS, Rho WY, Cho BR. Detection of Near-membrane Calcium Ions in Live Tissues with a Two-Photon Fluorescent Probe. Bull Kor Chem Soc. 2010; 31(3):599–605.
75. Kim MK, Lim CS, Hong JT, Han JH, Jang H-Y, Kim HM, Cho BR. Sodium-Ion-Selective Two-Photon Fluorescent Probe for In Vivo Imaging. Angew Chem Int Ed Engl. 2010; 49(2):364–367. [PubMed: 19998298]
76. Kim HM, Seo MS, An MJ, Hong JH, Tian YS, Choi JH, Kwon O, Lee KJ, Cho BR. Two-photon fluorescent probes for intracellular free zinc ions in living tissue. Angew Chem Int Ed Engl. 2008; 47(28):5167–5170. [PubMed: 18528837]
77. Lim CS, Kang DW, Tian YS, Han JH, Hwang HL, Cho BR. Detection of mercury in fish organs with a two-photon fluorescent probe. Chem Commun. 2010; 46(14):2388–2390.
78. Förster T. Diabatic and adiabatic processes in photochemistry. Pure Appl Chem. 1970; 24:443.
79. Weller A. Fast reactions of excited molecules. Prog React Kinet. 1961; 1:187.
80. Lawrence M, Marzzacco CJ, Morton C, Schwab C, Halpern AM. Excited state deprotonation of 2-naphthols by anions. J Phys Chem. 1991; 95(25):10294–10299.
81. Henary MM, Wu Y, Fahrni CJ. Zinc(II)-selective ratiometric fluorescent sensors based on inhibition of excited-state intramolecular proton transfer. Chem Eur J. 2004; 10(12):3015–3025. [PubMed: 15214085]

82. Henary MM, Fahrni CJ. Excited state intramolecular proton transfer and metal ion complexation of 2-(2′-hydroxyphenyl)benzazoles in aqueous solution. J Phys Chem A. 2002; 106(21):5210–5220.

83. Fahrni CJ, Henary MM, VanDerveer DG. Excited-state intramolecular proton transfer in 2-(2′-tosylaminophenyl)benzimidazole. J Phys Chem A. 2002; 106(34):7655–7663.

84. Taki M, Wolford JL, O'Halloran TV. Emission ratiometric imaging of intracellular zinc: design of a benzoxazole fluorescent sensor and its application in two-photon microscopy. J Am Chem Soc. 2004; 126(3):712–713. [PubMed: 14733534]

85. Tian YQ, Chen CI-Y, Yang C-C, Young AC, Jang S-H, Chen W-C, Jen AK-Y. 2-(2′-Hydroxyphenyl)benzoxazole-containing two-photon-absorbing chromophores as sensors for zinc and hydroxide ions. Chem Mater. 2008; 20(5):1977–1987.

86. Chen X-Y, Shi J, Li Y-M, Wang F-L, Wu X, Guo Q-X, Liu L. Two-photon fluorescent probes of biological Zn(II) derived from 7-hydroxyquinoline. Org Lett. 2009; 11(19):4426–4429. [PubMed: 19722549]

87. Stutzmann GE, LaFerla FM, Parker I. Ca(II) signaling in mouse cortical neurons studied by two-photon imaging and photoreleased inositol triphosphate. J Neurosci. 2003; 23(3):758–765. [PubMed: 12574404]

88. Ricken S, Leipziger J, Greger R, Nitschke R. Simultaneous measurements of cytosolic and mitochondrial Ca(II) transients in HT29 cells. J Biol Chem. 1998; 273(52):34961–34969. [PubMed: 9857027]

89. Szmacinski H, Gryczynski I, Lakowicz JR. Calcium-dependent fluorescence lifetimes of indo-1 for one-photon and 2-photon excitation of fluorescence. Photochem Photobiol. 1993; 58(3):341–345. [PubMed: 8234466]

90. Brust-Mascher I, Webb WW. Calcium waves induced by large voltage pulses in fish keratocytes. Biophys J. 1998; 75(4):1669–1678. [PubMed: 9746509]

91. Jones KT, Soeller C, Cannell MB. The passage of Ca(II) and fluorescent markers between the sperm and egg after fusion in the mouse. Development. 1998; 125(23):4627–4635. [PubMed: 9806912]

92. Chang CJ, Nolan EM, Jaworski J, Okamoto K-I, Hayashi Y, Sheng M, Lippard SJ. ZP8, a neuronal zinc sensor with improved dynamic range; Imaging zinc in hippocampal slices with two-photon microscopy. Inorg Chem. 2004; 43(21):6774–6779. [PubMed: 15476377]

93. Nolan EM, Jaworski J, Okamoto K-I, Hayashi Y, Sheng M, Lippard SJ. QZ1 and QZ2: Rapid, reversible quinoline-derivatized fluoresceins for sensing biological Zn(II). J Am Chem Soc. 2005; 127(48):16812–16823. [PubMed: 16316228]

94. Love R, Salazar G, Faundez V. Neuronal zinc stores are modulated by non-steroidal anti-inflammatory drugs: An optical analysis in cultured hippocampal neurons. Brain Research. 2005; 1061(1):1–12. [PubMed: 16242675]

95. Fisher JAN, Salzberg BM, Yodh AG. Near infrared two-photon excitation cross-sections of voltage-sensitive dyes. J Neurosic Methods. 2005; 148(1):94–102.

96. Makarov NS, Drobizhev M, Rebane A. Two-photon absorption standards in the 550–1600 nm excitation wavelength range. Opt Expr. 2008; 16(6):4029–4047.

97. Xu C, Webb WW. Measurement of two-photon excitation cross sections of molecular fluorophores with data from 690 to 1050 nm. J Opt Soc Am B - Opt Phys. 1996; 13(3):481–491.

98. Blab GA, Lommerse PHM, Cognet L, Harms GS, Schmidt T. Two-photon excitation action cross-sections of the autofluorescent proteins. Chem Phys Lett. 2001; 350(1–2):71–77.

99. Huang SH, Heikal AA, Webb WW. Two-photon fluorescence spectroscopy and microscopy of NAD(P)H and flavoprotein. Biophys J. 2002; 82(5):2811–2825. [PubMed: 11964266]

100. Kierdaszuk B, Malak H, Gryczynski I, Callis P, Lakowicz JR. Fluorescence of reduced nicotinamides using one- and two-photon excitation. Biophys Chem. 1996; 62(1–3):1–13. [PubMed: 8962467]

101. Rothstein EC, Carroll S, Combs CA, Jobsis PD, Balaban RS. Skeletal muscle NAD(P)H two-photon fluorescence microscopy in vivo: Topology and optical inner filters. Biophys J. 2005; 88(3):2165–2176. [PubMed: 15596503]

102. Masters BR, So PTC, Gratton E. Multiphoton excitation fluorescence microscopy and spectroscopy of in vivo human skin. Biophys J. 1997; 72(6):2405–2412. [PubMed: 9168018]

103. Shaner NC, Steinbach PA, Tsien RY. A guide to choosing fluorescent proteins. Nat Methods. 2005; 2(12):905–909. [PubMed: 16299475]
104. Giepmans BNG, Adams SR, Ellisman MH, Tsien RY. Review - The fluorescent toolbox for assessing protein location and function. Science. 2006; 312(5771):217–224. [PubMed: 16614209]
105. Kamiya M, Johnsson K. Localizable and highly sensitive calcium indicator based on a BODIPY fluorophore. Anal Chem. 2010; 82(15):6472–6479. [PubMed: 20590099]
106. Bannwarth M, Correa IR, Sztretye M, Pouvreau S, Fellay C, Aebischer A, Royer L, Rios E, Johnsson K. Indo-1 derivatives for local calcium sensing. ACS Chem Biol. 2009; 4(3):179–190. [PubMed: 19193035]
107. Tomat E, Nolan EM, Jaworski J, Lippard SJ. Organelle-Specific Zinc Detection Using Zinpyr-Labeled Fusion Proteins in Live Cells. J Am Chem Soc. 2008; 130(47):15776–15777. [PubMed: 18973293]
108. Keppler A, Pick H, Arrivoli C, Vogel H, Johnsson K. Labeling of fusion proteins with synthetic fluorophores in live cells. Proc Natl Acad Sci USA. 2004; 101(27):9955–9959. [PubMed: 15226507]
109. Keppler A, Gendreizig S, Gronemeyer T, Pick H, Vogel H, Johnsson K. A general method for the covalent labeling of fusion proteins with small molecules in vivo. Nat Biotechnol. 2003; 21(1): 86–89. [PubMed: 12469133]
110. Los GV, Encell LP, McDougall MG, Hartzell DD, Karassina N, Zimprich C, Wood MG, Learish R, Ohane RF, Urh M, Simpson D, Mendez J, Zimmerman K, Otto P, Vidugiris G, Zhu J, Darzins A, Klaubert DH, Bulleit RF, Wood KV. HatoTag: A novel protein labeling technology for cell imaging and protein analysis. ACS Chem Biol. 2008; 3(6):373–382. [PubMed: 18533659]
111. Larson DR, Zipfel WR, Williams RM, Clark SW, Bruchez MP, Wise FW, Webb WW. Water-soluble quantum dots for multiphoton fluorescence imaging in vivo. Science. 2003; 300(5624): 1434–1436. [PubMed: 12775841]
112. Liu CL, Ho ML, Chen YC, Hsieh CC, Lin YC, Wang YH, Yang MJ, Duan HS, Chen BS, Lee JF, Hsiao JK, Chou PT. Thiol-functionalized gold nanodots: Two-photon absorption property and imaging in vitro. J Phys Chem C. 2009; 113(50):21082–21089.
113. Patel SA, Richards CI, Hsiang JC, Dickson RM. Water-soluble Ag nanoclusters exhibit strong two-photon-induced fluorescence. J Am Chem Soc. 2008; 130(35):11602–11603. [PubMed: 18686957]
114. Ramakrishna G, Varnavski O, Kim J, Lee D, Goodson T. Quantum-sized gold clusters as efficient two-photon absorbers. J Am Chem Soc. 2008; 130(15):5032–5033. [PubMed: 18357982]

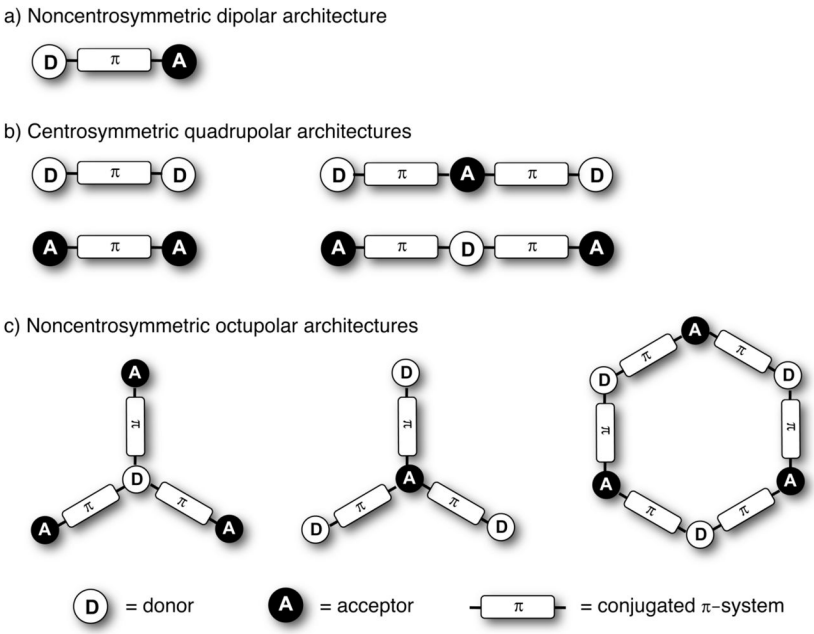

Figure 1.
Selection of molecular architectures for the design of fluorophores with large two-photon absorption cross sections.

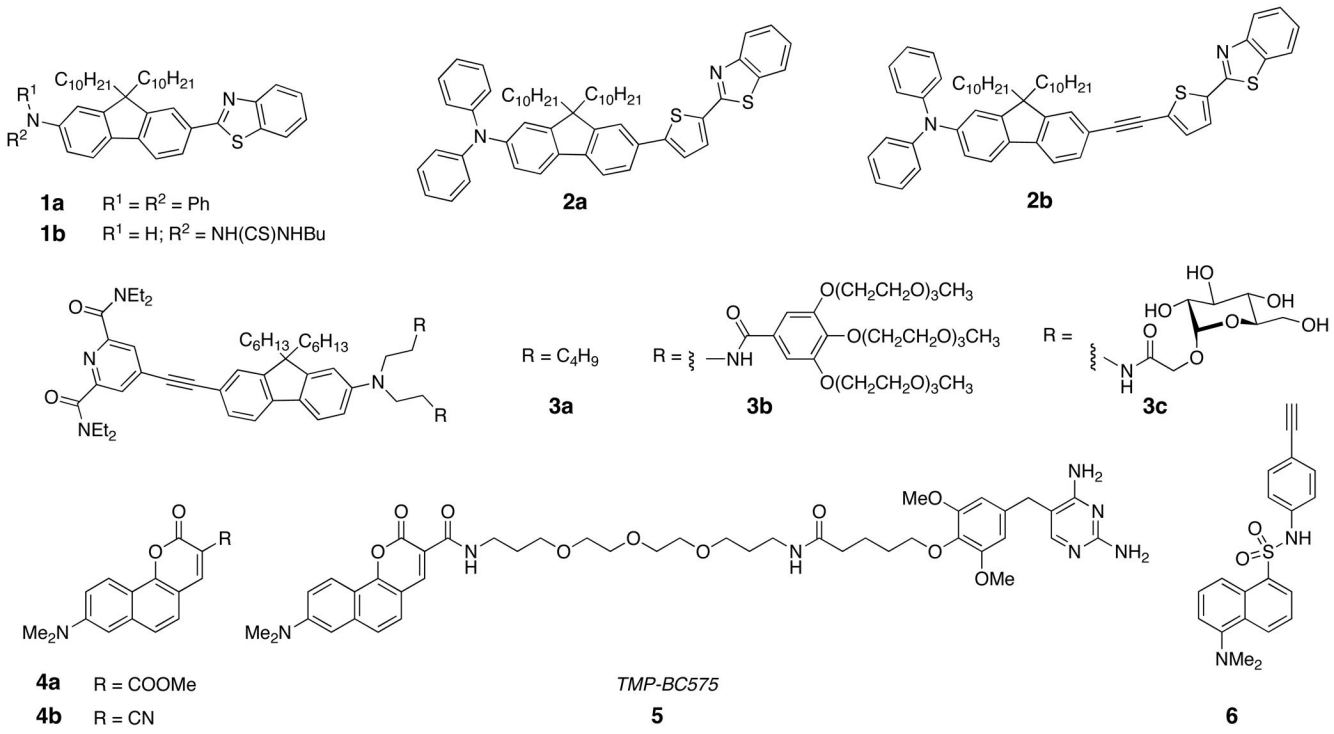

Figure 2.

Fluorescent labels with dipolar architecture developed for biological two-photon imaging. Selected photophysical properties of each dye are compiled in Table 1.

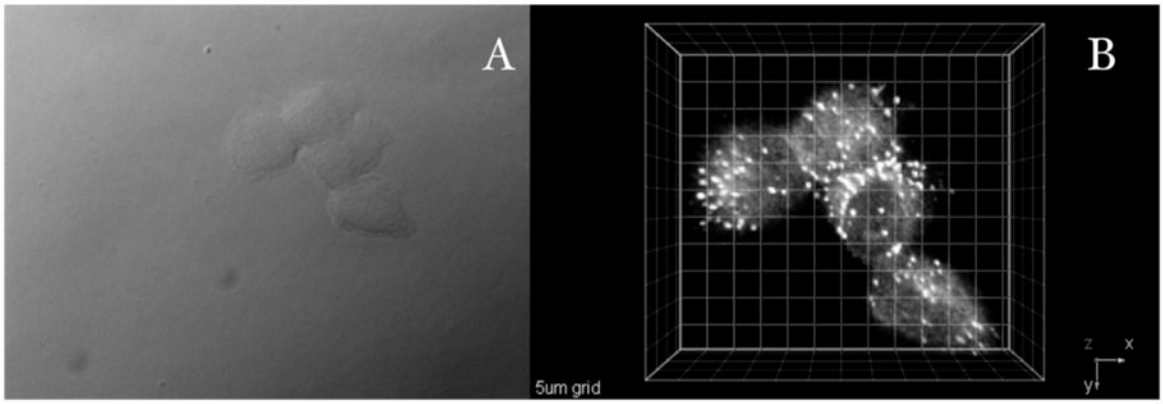

Figure 3.

Two-photon fluorescence micrograph of HCT 116 cells incubated with probe **2a** (20 μM, 1 h 50 min). (A) DIC and (B) 3D reconstruction from overlaid TPEM images obtained from a modified laser scanning confocal microscopy system equipped with a broadband, tunable Ti:sapphire laser (220 fs pulse width, 76 MHz repetition rate), pumped by a 10 W frequency doubled Nd:YAG laser. (60X objective, NA = 1.35). Scale: 5 μm grid. Reprinted with permission from ref. Copyright American Chemical Society 2010.

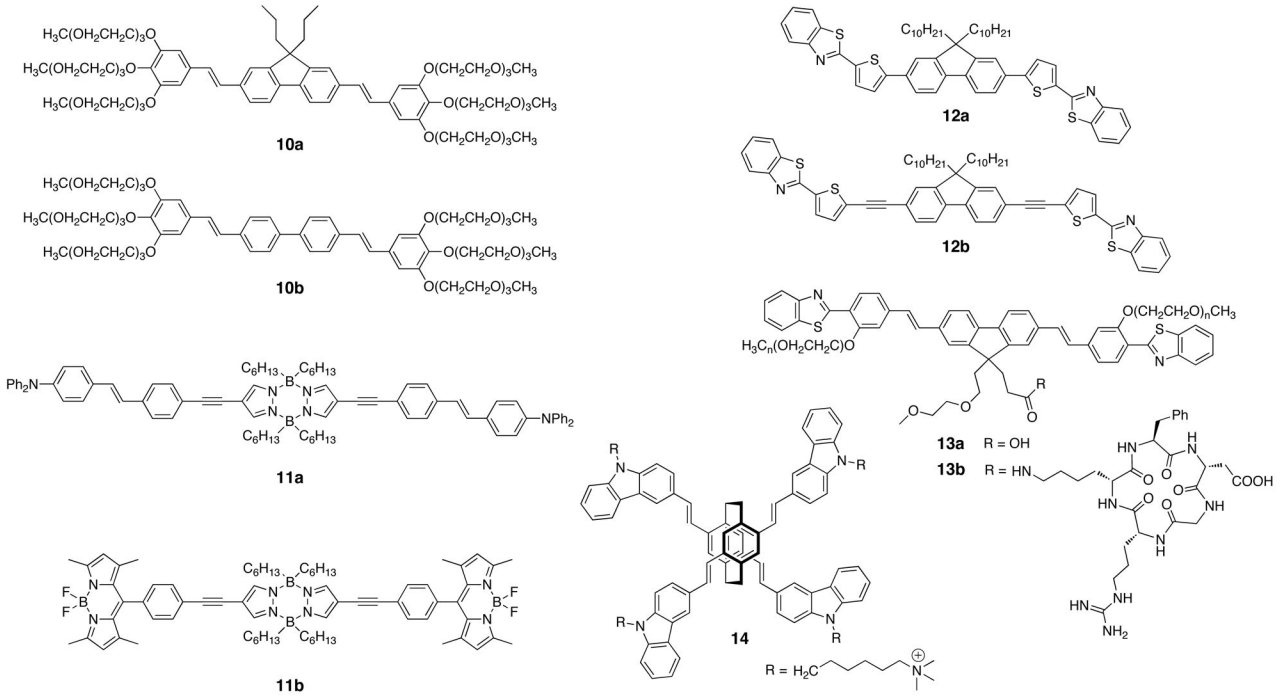

Figure 4.

Fluorescent labels with quadrupolar architecture developed for biological two-photon imaging. Selected photophysical properties of each dye are compiled in Table 2.

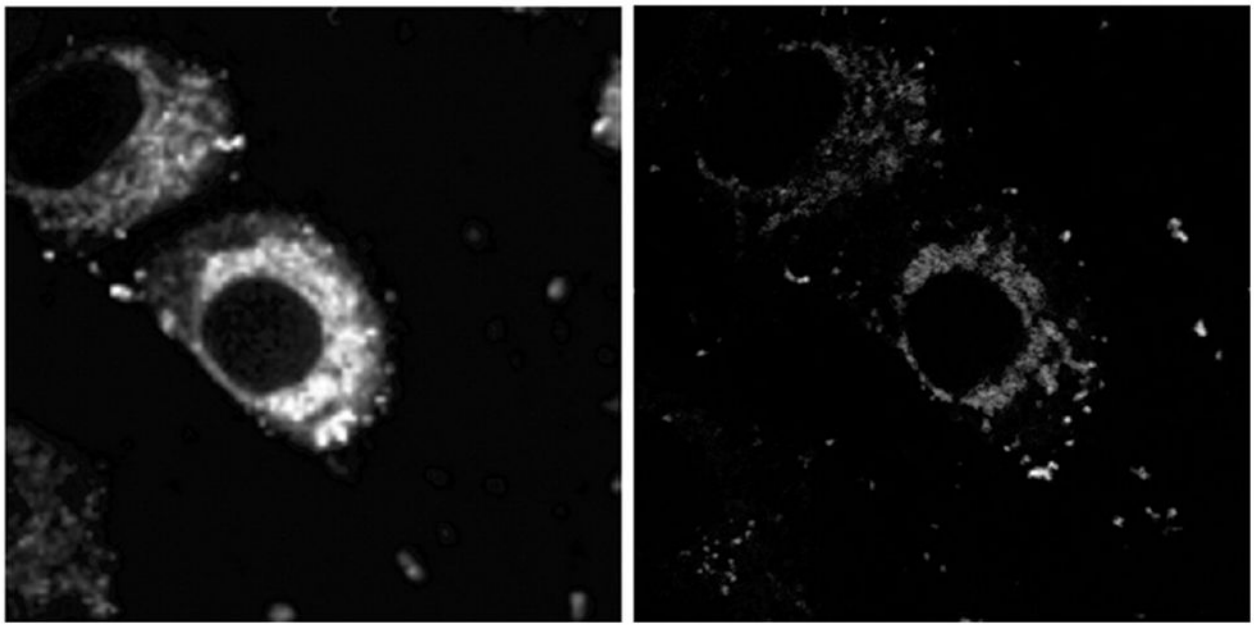

Figure 5.

Two-photon images of HeLa cells stained with **11a** (left, 800 nm, 1 mW), and **11b** (right, 900 nm, 15 mW). Reprinted with permission from ref. Copyright American Chemical Society 2009.

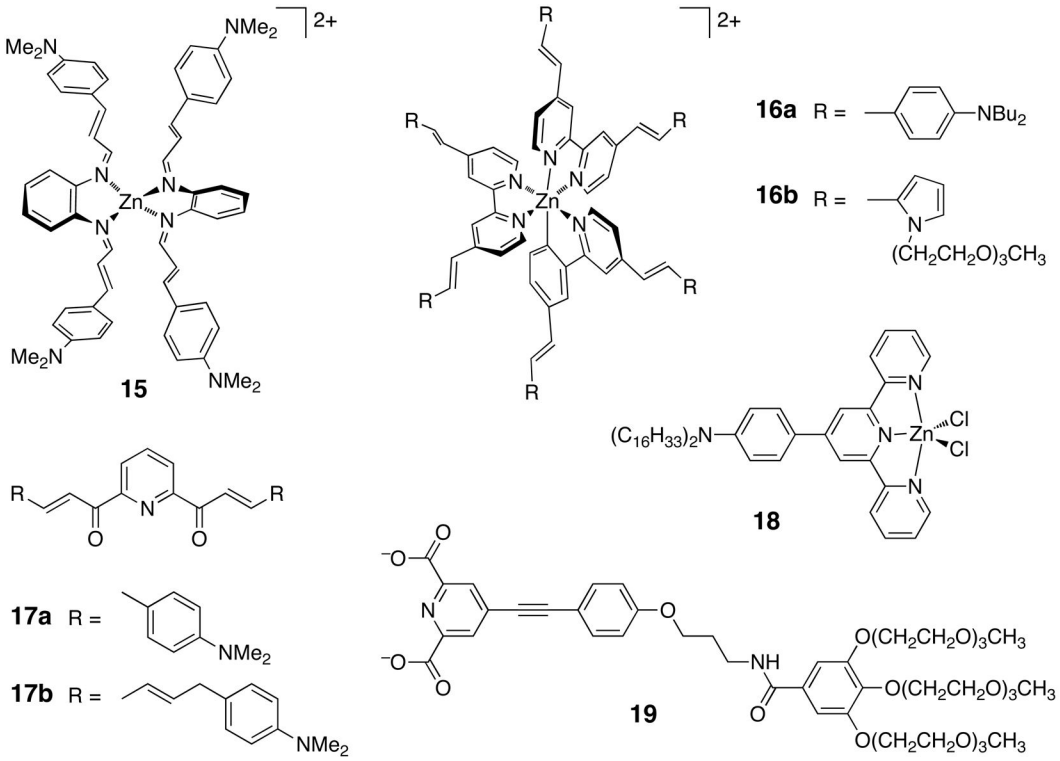

Figure 6.
Metal complexes with octupolar fluorophore architecture with strongly enhanced 2PA cross sections.

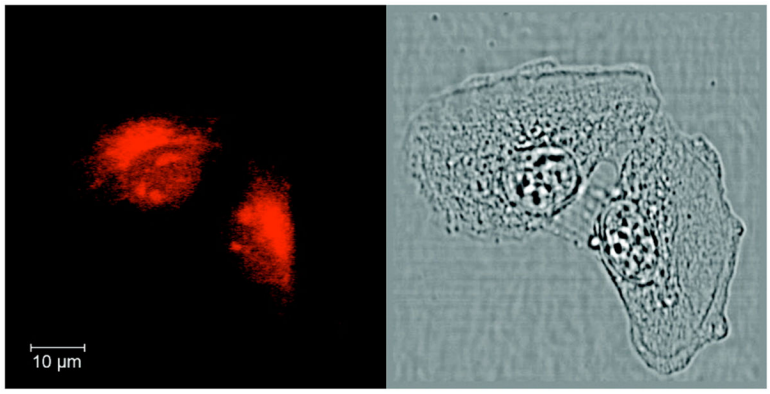

Figure 7.

Two-photon excited luminescence (left, excitation at 760 nm) and phase contrast (right) images of T24 cancer cells fixed in ethanol and loaded with $[Na]_3[Eu(\mathbf{19})_3]$. Images were taken on a Zeiss LSM510 NLO META confocal microscope equipped with a femtosecond Ti:sapphire laser. Reprinted with permission from ref. Copyright American Chemical Society 2008.

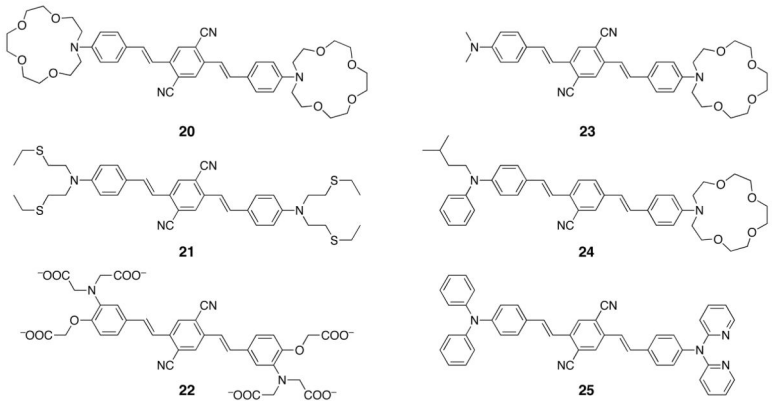

Figure 8.

Metal-responsive fluorescent two-photon absorbing indicators with quadrupolar architecture. Selected photophysical properties of each dye are compiled in Table 3.

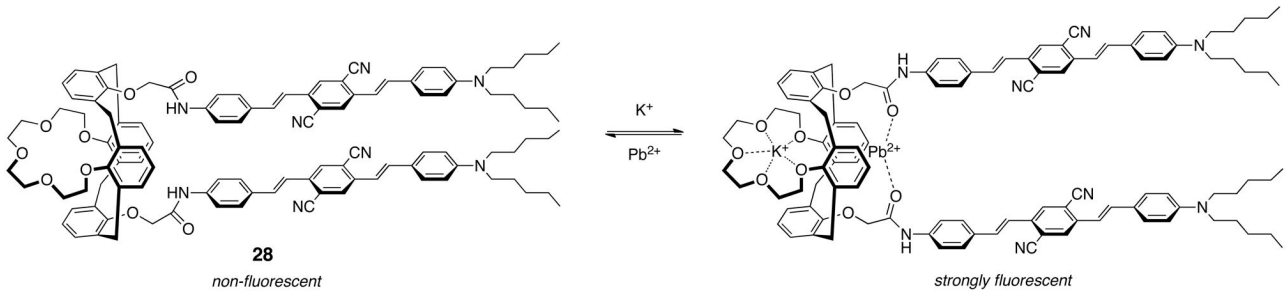

Figure 9.

Fluorescence switching with a pair of centrosymemtric fluorophores. The free probe **28** is quenched through resonance energy transfer. Coordiantion of K(I) allosterically renders the conformation of the probe more favorable for Pb(II) binding, which inhibits fluorescence quenching through an additional conformational change.

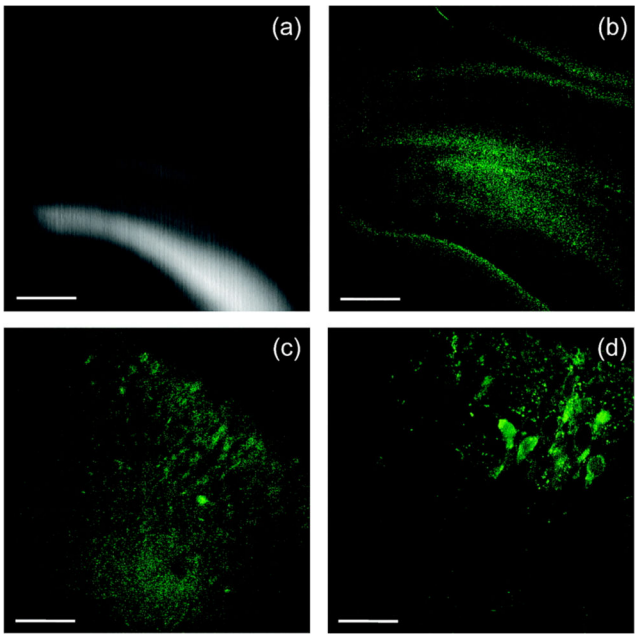

Figure 10.

Images of a fresh mouse hippocampal slice stained with 10 μM **35 (**AM ester, CMg1-AM). (a) A bright-field image (a) and TPEM image (b) show the dentate gyrus and the CA1 region at a depth of 250 μm by magnification at 10×. (c) Magnification at 40× shows the CA1 layer at a depth of 100 μm. (d) Magnification at 100× shows CA1 pyramidal neurons at a depth of 100 μm. Scale bars: 300 (a, b), 120 (c), and 30 (d) μm, respectively. The TPEM images were collected at 560–640 nm upon excitation by 880 nm laser photons. Reprinted with permission from ref. Copyright American Chemical Society 2007.

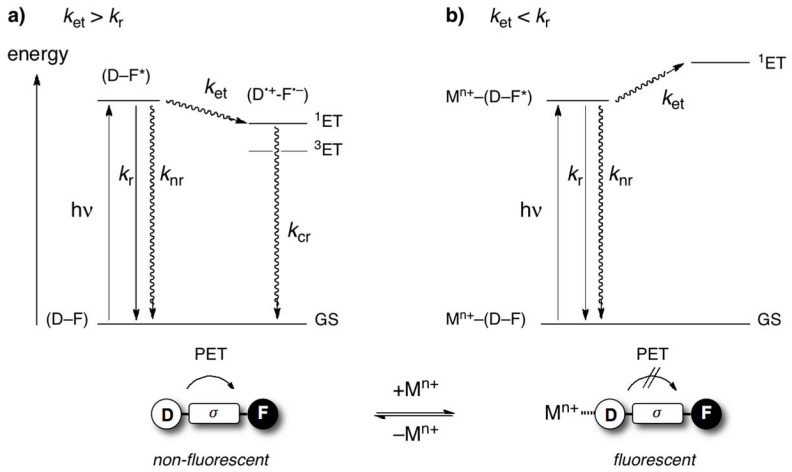

Figure 11.

Photoinduced electron transfer (PET) switching. a) In absence of the metal cation M^{n+}, electron transfer from the donor D to the excited fluorophore (F*) is thermodynamically favorable. The rate constant for electron transfer k_{et} is faster than k_r for radiative deactivation, resulting in emission quenching. b) Metal coordination to the electron donor D decreases the driving force for PET, and slows down the electron transfer process. Radiative deactivation favorably competes with PET, and the fluorescence is switched on (k_{nr} = non-radiative deactivation rate constant, k_{cr} = charge recombination rate constant).

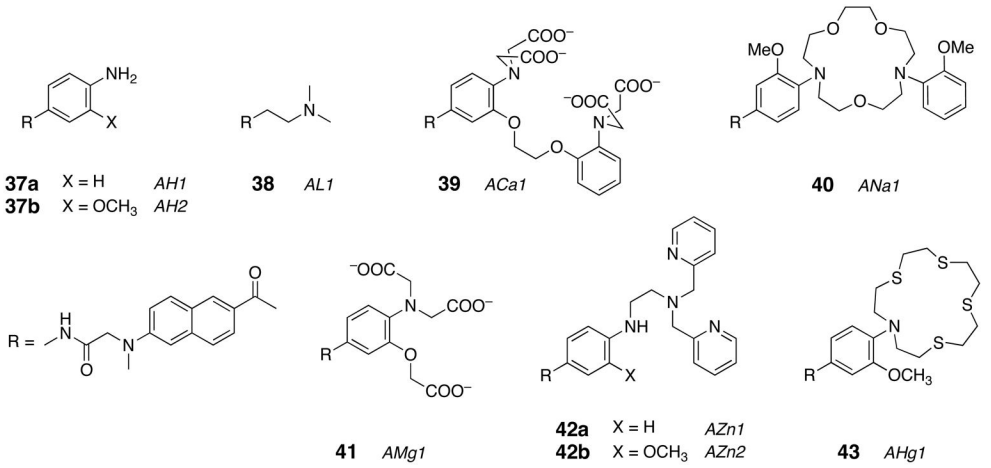

Figure 12.

Chemical structures of cation-responsive indicators utilizing a dipolar naphthalene moiety as two-photon absorbing fluorophore. The fluorescence output is modulated in an analyte-dependent manner through a photoinduced electron transfer (PET) switching mechanism.

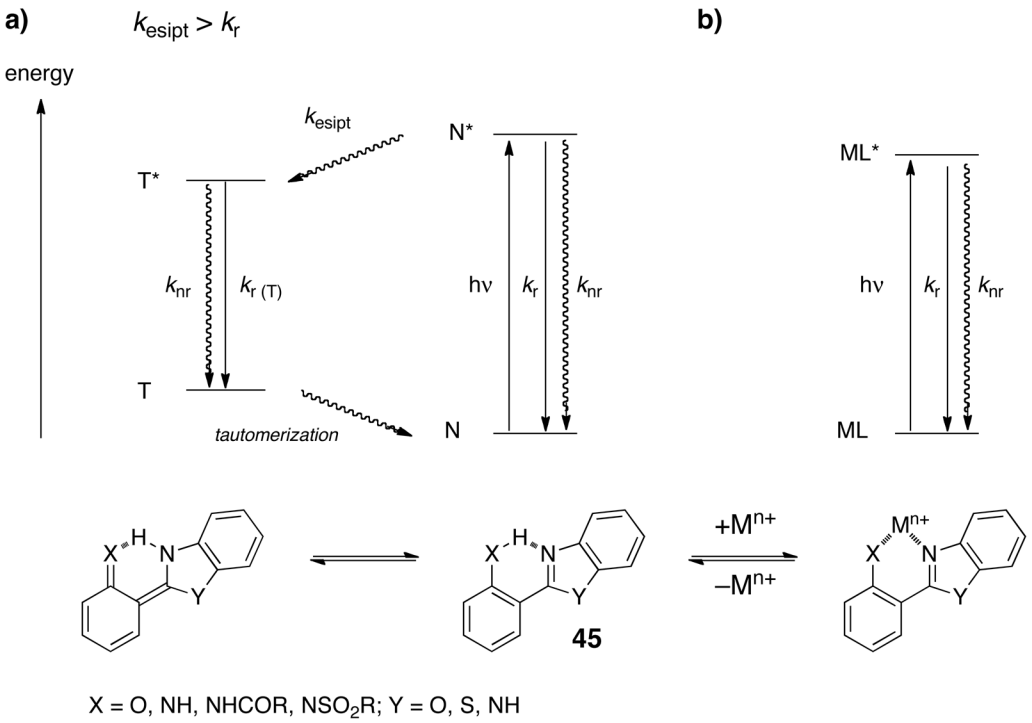

Figure 13.

Simplified Jablonski diagram illustrating metal ion induced inhibition of excited state intramolecular proton transfer (ESIPT). a) Light absorption leads to formation of a locally excited state N*, which undergoes ultrafast intramolecular proton transfer (ESIPT) to form the excited tautomer T*. After radiative deactivation, the tautomer thermally equilibrates back to the initial ground state N. b) Metal coordination inhibits ESIPT due to removal of the intramolecular hydrogen bond. The fluorescence emission is strongly blue-shifted compared to the metal free indicator. (k_r = radiative rate constant, k_{nr} = non-radiate rate constant, k_{ESIPT} = rate constant for excited state intramolecular proton transfer).

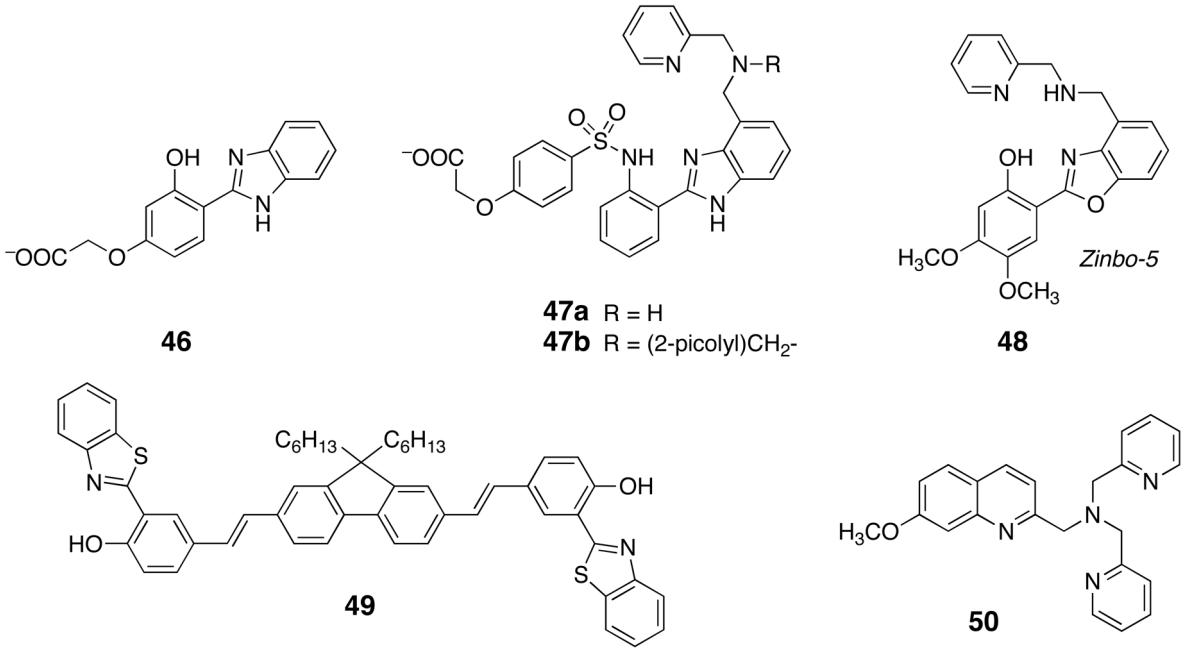

Figure 14.

Chemical structures of cation-responsive indicators utilizing an excited state intramolecular proton transfer (ESIPT) process to alter the fluorescence output in a metal-ion dependent fashion.

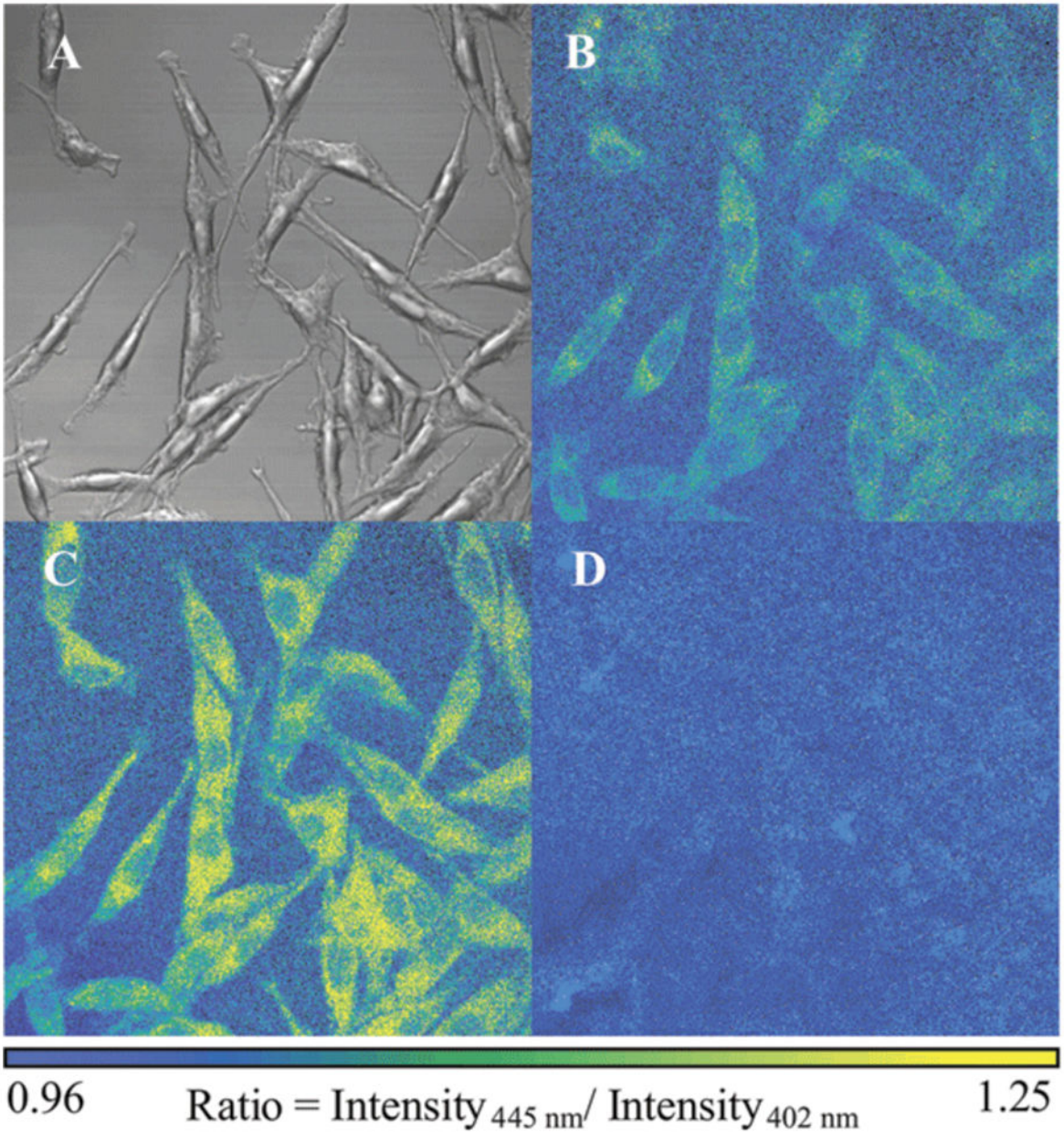

Figure 15.

TPEM emission ratio images of fibroblast [L(TK)$^-$] cells incubated with **48** (Zinbo-5). (A) Brightfield transmission image; (B) TPEM ratio of images collected at 445 and 402 nm; (C) TPEM ratio image following a 30 min treatment with 10 μM zinc sulfate and 20 μM pyrithione at pH 7.4, 25 °C, followed by wash with **48** stock; (D) TPEM ratio image of the same field after a 15 min treatment with 1 mM TPEN. Reprinted with permission from ref. Copyright American Chemical Society 2004.

Table 1

Photophysical properties of fluorescent labels with dipolar architecture developed for biological two-photon imaging (structures depicted in Figure 2).

Fluorophore	2PA Cross Section (δ) [GM]	Action Cross Section (ηδ) [GM]	Φ_F[a]	abs λ_{max} [nm]	2PA λ_{max} [nm]	em λ_{max} [nm]	Solvent	Reference
1a	202	120	0.60	390	780	492	CH_2Cl_2	
1b	25	19	0.74	363	740	475	DMSO	
2a	248	213	0.86	403	730	452	hexane	
2b	563	518	0.92	398	730	444	hexane	
3a	1146	1020	0.89	411	830	525	CH_2Cl_2	
4a	350	67	0.19	453	880	570	water	
4b	470	24	0.05	457	940	590	water	
6	92	n.d.	0.49[b]	350[b]	720	538	DMSO	

[a] Fluorescence quantum yield.

[b] dichloromethane as solvent.

Chem Mater. Author manuscript; available in PMC 2017 May 12.

Table 2

Photophysical properties of fluorescent labels with centrosymmetric architecture developed for biological two-photon imaging (structures depicted in Figure 4).

Fluorophore	2PA Cross Section (δ) [GM]	Action Cross Section (ηδ) [GM]	Φ_F [a]	abs λ_{max} [nm]	2PA λ_{max} [nm]	em λ_{max} [nm]	Solvent	Reference
10a	160	115	0.72	383	720	453	water	,
10b	110	43	0.39	357	720	450	water	,
11a	100	57	0.57	387	740	479	dichloromethane	
11b	314	125	0.40	502	800	512	dichloromethane	
12a	335	328	0.98	405	730	446	hexane	
12b	1090	1035	0.95	397	730	433	hexane	
13a	100–1000	50–500	0.50	432	690–800	509	water	
14	700	294	0.42	410	700	505	water	

[a]Fluorescence quantum yield.

Table 3

Fluorescent metal-ion indicators with centrosymmetric architecture

Fluorophore	2PA Cross Section (δ).[GM]	Action Cross Section (ηδ).[GM]	Φ_F [a]	abs λ_{max} [nm]	2PA λ_{max} [nm]	em λ_{max} [nm]	Solvent	Reference
20	2150	430	0.20	472	810	610	acetonitrile	
20+Mg(II)	45	9	0.19	378	810	576	acetonitrile	
21	1120	570	0.50	467	810	590	acetonitrile	
21+Ag(I)	300	n/a	n.d.	447	810	n/a	acetonitrile	
22	517	62	0.12	362	720	460	HEPES pH 7.2	
22+Pb(II)	638	51	0.08	362	720	590	HEPES pH 7.2	
23	1800	180	0.10	468	810	624	acetonitrile	
23+Mg(II)	300	9	0.03	445	810	665	acetonitrile	
24	120	56	0.47	425	760	550	acetonitrile	
24+Ca(II)	20	n.d.	n.d.	425	820	550	acetonitrile	
25	30	14	0.47	425	780	610	acetonitrile	
25+Zn(II)	n.d.	4	n.d.	425	780	n.d.	acetonitrile	
26a	133	36	0.35	370	800	440	DMF	
26b	917	110	0.12	434	800	564	DMF	
27	12	n.d.	n.d.	362	700	510	HEPES pH 7.0	,
27+Ca(II)	11	n.d.	n.d.	335	700	512	HEPES pH 7.0	,
28	n.d.	n.d.	0.017	460	780	520	acetonitrile	
28+Pb(II)+K(I)	998	100	0.1	385	780	500	acetonitrile	

[a] Fluorescence quantum yield.

Table 4

Fluorescent metal-ion indicators with dipolar architecture

Fluorophore	Two-photon Cross Section (δ).[GM]	Action Cross Section (ηδ).[GM]	Φ_F [a]	abs λ_{max} [nm]	2PA λ_{max} [nm]	em λ_{max} [nm]	Solvent	Reference
29	350	112	0.32	400	820	609	ethanol	
29-Zn(II)	240	122	0.51	385	820	542	ethanol	
29-Hg(II)	350	161	0.46	382	820	540	ethanol	
30	130	108	0.83	391	780	496	THF	
30-Zn(II)	65	47	0.73	381	780	462	THF	
31	840	168	0.20	400	790	613	water	
32	31	11	0.35	338	690	441	MeOH	
32-Zn(II)	77	55	0.71	362	730	497	MeOH	
33a (pH 3)	60	42	0.7	355	710	530	aq. buffer	
33a (pH 8)	15	12	0.8	326	710	465	aq. buffer	
33b (pH 2)	65	19.5	0.3	390	800	569	aq. buffer	
33b (pH 12)	5	2.5	0.5	332	710	472	aq. buffer	
34a (pH 2)	40	4	0.1	381	780	562	aq. buffer	
34a (pH 12)	20	14	0.7	328	710	450	aq. buffer	
34b (pH 2)	35	1.8	0.05	382	780	572	aq. buffer	
34b (pH 12)	20	14	0.7	330	710	450	aq. buffer	
35	290	84	0.29	413	820	556	water	
35-Mg(II)	382	107	0.28	443	880	559	water	

[a]Fluorescence quantum yield.

Table 5

Fluorescent metal-ion indicators with PET switching mechanism

Fluorophore	Two-photon Cross Section (δ).[GM]	Action Cross Section (ηδ). [GM]	Φ_F [a]	Fluorescence enhancement factor	abs λ_{max} [nm]	2PA λ_{max} [nm]	em λ_{max} [nm]	Solvent	Reference
37a-H^+	143	86	0.60	22	364	780	498	pH 3	
37b-H^+	138	88	0.64	64	365	780	496	pH 3	
38	127	92	0.72	n/a	364	780	496	pH 3	
39-Ca(II)	224	110	0.49	40	369	780	500	pH 7.2	
40-Na(I)	146	95	0.65	8	365	780	500	pH 7.1	
41-Mg(II)	215	125	0.58	15	365	780	498	pH 7.1	
42a-Zn(II)	210	86	0.47	21	365	780	498	pH 7.2	
42b-Zn(II)	140	95	0.65	54	365	780	499	pH 7.2	
43-Hg(II)		110	0.15	6	361	780	498	pH 7.0	
44a-Ca(II)		90	0.043	12	372	780	500	pH 7.0	
44b-Ca(II)		100	0.16	8	357	780	501	pH 7.0	

[a] Fluorescence quantum yield.

Table 6

Two-photon cross sections of selected fluorophores commonly used in biological research.

Fluorophore	Two-photon Cross Section (δ).[GM]	Action Cross Section (ηδ).[GM]	abs λ_{max} [nm]	2PA λ_{max} [nm]	em [nm] λ_{max}	Reference
Fluorescent Labels:						
Fluorescein, pH 13	37		491	780	514	
BODIPY		17	507	920	520	
Nile Blue A	0.6		649[a]	800	660[a]	
Lucifer Yellow	2.6		430	850	530	
Rhodamine 6G	55		530[b]	750	558[b]	
Rhodamine B	180		543[b]	850	568[b]	
Coumarin 485	35		403[b]	750	501[b]	
Fluorescent Indicators:						
Fura-2		11	362	700	518	
with Ca(II)		12	335	700	510	
C18-fura-2 with Ca(II)		36	335	780	505	
Indo-1		3.5	349	700	482	
with Ca(II)	2.1	1.5	331	700	398	
Indo-1	12	4.5		700		
Calcium Green		2	508	820	534	
with Ca(II)		30	508	820	534	
Mag-fura2 with Mg(II)	56	17	530	780	491	
Lysotracker	125	10	575	780	593	
SBFI Na	250	20	334	780	524	
Sodium Green with Na(I)	150	30	507	800	530	
FluoZin with Zn(II)	55	24	494	780	516	
TSQ with Zn(II)	10	4	362	780	495	
Endogenous Fluorophores:						

Fluorophore	Two-photon Cross Section (δ).[GM]	Action Cross Section (ηδ).[GM]	abs λ_{max} [nm]	2PA λ_{max} [nm]	em [nm] λ_{max}	Reference
NADH	0.02		340	690–730	450	
Flavins	0.1–0.8		375, 445	700–730	526	
EGFP	41		489	920	508	
DsRed	11		558	960	583	

[a] in octanol.

[b] in methanol.